catalysts

MDPI

*Article*

# Banana (*Musa sapientum*) Waste-Derived Biochar–Magnetite Magnetic Composites for Acetaminophen Removal via Photochemical Fenton Oxidation

**Manasik M. Nour [1], Maha A. Tony [2,3], Mai Kamal Fouad [4] and Hossam A. Nabwey [1,*]**

[1] Department of Mathematics, College of Science and Humanities in Al-Kharj, Prince Sattam bin Abdulaziz University, Al-Kharj 11942, Saudi Arabia
[2] Basic Engineering Science Department, Faculty of Engineering, Menoufia University, Shebin El-Kom 32511, Egypt; dr.maha.tony@gmail.com
[3] Advanced Materials/Solar Energy and Environmental Sustainability (AMSEES) Laboratory, Faculty of Engineering, Menoufia University, Shebin El-Kom 32511, Egypt
[4] Chemical Engineering Department, Faculty of Engineering, Cairo University, Giza, Egypt
* Correspondence: h.mohamed@psau.edu.sa

## Abstract

Recently, researchers have been focused on the recycling as well as transforming of bio-waste streams into a valuable resource. Banana peels are promising for such application, due to their wide availability. In this context, the integration of banana peel-derived biochar with environmentally benign magnetite has significantly broadened its potential applications as a solar photocatalyst compared to the conventional photocatalysts. The materials are mixed in varied proportions of Ban-Char500-Mag@-(0:1), Ban-Char500@Mag-(1:1) and Ban-Char500@Mag-(2:1) and characterized using X-ray diffraction (XRD) and scanning electron microscopy (SEM) augmented with dispersive X-ray spectroscopy (EDX). Such modification is leading to an improvement in its application as a solar photocatalyst using the photochemical solar collector facility. The study discusses the factors controlling acetaminophen removal from aqueous effluent within 30 min of solar illumination time. Furthermore, the highlighted optimum parameters are pH 3.0, using 10 mg/L of the Ban-Char500@Mag-(1:1) catalyst and 100 mg/L of the hydrogen peroxide as a Fenton combination system for removing a complete acetaminophen from wastewater (100% oxidation). Also, the temperature influence in the oxidation system is studied and the high temperature is unfavorable, which verifies that the reaction is exothermic in nature. The catalyst is signified as a sustainable (recoverable, recyclable and reusable) substance, and showed a 72% removal even though it was in the six cyclic uses. Further, the kinetic study is assessed, and the experimental results revealed the oxidation process is following the first-order kinetic reaction. Also, the kinetic–thermodynamic parameters of activation are investigated and it is confirmed that the oxidation is exothermic and non-spontaneous in nature.

**Keywords:** acetaminophen; photocatalysis; Fenton; solar energy; banana peels

Academic Editor: Enric Brillas

Received: 16 August 2025
Revised: 26 September 2025
Accepted: 4 October 2025
Published: 5 October 2025

**Citation:** Nour, M.M.; Tony, M.A.; Fouad, M.K.; Nabwey, H.A. Banana (*Musa sapientum*) Waste-Derived Biochar–Magnetite Magnetic Composites for Acetaminophen Removal via Photochemical Fenton Oxidation. *Catalysts* **2025**, *15*, 955. https://doi.org/10.3390/catal15100955

## 1. Introduction

Globally, rapid industrial growth has been accompanied by a substantial increase in water consumption, resulting in massive discharges of wastewater from various industrial activities [1,2]. Among these, the pharmaceutical industry is one of the fastest expanding sectors [3,4]. Pharmaceuticals encompass a wide range of compounds, including antibiotics, anti-inflammatory drugs, lipid regulators, and other therapeutic agents [5–11]. The discharge of pharmaceuticals into aquatic systems is particularly concerning, as they are increasingly recognized as emerging pollutants (EPs) due to their low biodegradability, high persistence, and potential for bioaccumulation [12–16]. Pharmaceutical effluents are released at different stages of their life cycle [17,18], from production to disposal, and their persistence in aquatic environments poses risks to both human health and ecosystems [19–27]. Consequently, considerable research efforts have been directed toward addressing these emerging pollutants [28–33]. Various treatment strategies—such as advanced oxidation processes, flotation, electrochemical techniques, and biological methods—have been proposed to mitigate pharmaceutical contamination in aquatic ecosystems [34–39]. However, many of these approaches face limitations, including high operational and maintenance costs, as well as the potential formation of secondary toxic by-products.

The existence of pharmaceuticals is widespread in the modern societies as emerging chemicals [15–19], and could be as a result of several activities [20–27]. Therefore, such pharmaceutical effluent discharge is a challenge, from their production to their elimination [26–28]. Moreover, their presence in the aqueous system is a global issue that might cause damage to human beings as well as numerous wildlife species [29,31]. Hence, ever-increasing efforts have been devoted to enable the emergence of those EPs [32]. Various systems have been suggested to treat such pharmaceuticals contaminating the ecosystem, such as oxidation, flotation, electrochemical techniques and biological managements [33,34]. Nevertheless, such methods are not convenient because of expensive operating or maintenance charges or generating secondary excess toxic contaminants.

Advanced oxidation processes (AOPs) are promising treatment candidates due to their advantages, including simple operation, cost-effectiveness, and high efficiency in both removing and mineralizing pollutants [35–42]. The current compilation in research is looking for sustainable treatment facilities to better signify the frontiers in such a field [17,39]. Fenton oxidation, which uses iron oxides, is suitable for AOP treatment because pollutants can be oxidized and completely mineralized into harmless end products, such as carbon dioxide and water, upon activation with $H_2O_2$. However, although the reaction commonly requires a relatively short reaction time, homogenous Fenton process forms iron sludge as a secondary pollutant, and it is essential to deal with it prior to final disposal [43]. Further, not only is such sludge a drawback, but also the acidic pH, losing the iron activity and thereby reducing the oxidation efficiency [44,45]. To avoid such parameters that hinder the system and to attain a high removal efficiency, solar radiation might be combined with the Fenton oxidation to increase the system activity and reach a higher mineralization compared to the solo Fenton treatments. It is noteworthy that the operational cost of the Fenton system can be reduced by using renewable solar energy [46]. To sum up, chemical precursors of the Fenton system are still behind the cost of the process.

Nevertheless, most published studies on the Fenton reaction do not utilize waste-derived materials as a catalyst source. This gap highlights the novelty of the present work, where waste is utilized as a functional material and applied for wastewater remediation, thereby promoting sustainable resource use. Thus, to reach an economic sustainable Fenton oxidation using waste sources as an ecological catalyst source coupled with magnetite nanoparticles is essential for a substitute of metal oxides that is signified as the backbone of the Fenton reaction [47,48]. Banana peels (*Musa sapientum*) generated in millions of tons

annually as agro-industrial by-products from beverage factories, local shops, and households, represent a significant waste challenge [49–51]. Although various techniques are dealing with such banana peel management, the common handling facility is dumping or landfilling, so as to be an organic fertilizer, or may be to be used as animal feed [11,52,53,54]. Converting banana peels into functional catalysts offers a win–win strategy to simultaneously address solid waste management and water pollution

In this work, we introduce a novel approach that integrates naturally abundant agricultural waste with magnetite to create a recyclable catalyst for solar photo-Fenton applications. Specifically, biochar derived from *Musa sapientum* was functionalized with environmentally benign magnetite via a simple co-precipitation route. This hybrid material, serving as a cost-effective and sustainable photocatalyst, was thoroughly characterized and subsequently applied for the oxidation of acetaminophen in wastewater. The novelty of this study lies in the synergistic utilization of waste-derived biochar, its integration with magnetite, and the solar collector that assisted photo-Fenton processes to enhance solar energy harvesting for efficient pharmaceutical wastewater remediation.

## 2. Results and Discussion

### *2.1. Structural and Morphological Characterization of Ban-Char500 Samples*

XRD

XRD, X-ray diffraction patterns of magnetite and composite magnetite/biochar are displayed in Figure 1. As exhibited in Figure 1a, the magnetite crystal structure XRD data (JCPDS No. 89-4319) [14] appears in the pattern. The XRD pattern exhibits well-defined sharp diffraction peaks. The peaks appear at the 2θ values of 30.15, 35.61, 43.20, 57.71, and 62.81, which correspond to the plans of (220), (311), (400), (422), and (620), respectively. Also, it is noteworthy to mention that the most intensive magnetite peaks appear in the two samples of (b) Char500@Mag-(1:1) and (d) Ban-Char500@Mag-(2:1), with well-defined sharp diffraction peaks that exhibit good crystalline phase. That verifies the well distributed magnetite nanoparticles in the composites, without causing damage to the magnetite nanoparticle crystal structure. However, XRD examination of the composite containing banana biochar, (b) Ban-Char500@Mag-(1:1), (c) Ban-Char500@Mag-(2:1) and (d) Ban-Char500@Mag-(1:0) reveals broad peaks indicative of an amorphous carbon layer, suggesting the predominantly amorphous nature of the banana peel material. Furthermore, the inclusion of banana peel into magnetite mostly does not result in alterations to the crystallinity or phase of the magnetite material. However, an observable change is evident in the introduction of banana biochar into the magnetite material consequences in a reduction in peak intensity within the XRD pattern of the composite of Ban-Char500@Mag-(1:1) or Ban-Char500@Mag-(2:1) materials. This could be due to the fact that banana biochar, which is signified as a carbon-based material, does not reveal diffraction peaks in XRD patterns [4]. As peak intensity in XRD patterns reflects the extent of diffraction at a specific angle, the addition of banana biochar to magnetite in different proportions could potentially reduce the concentration of magnetite in the material campsite, due to the mixing ratios, thereby leading to a deduction in the peak intensity represented in the XRD pattern [4–6]. Additionally, the XRD pattern of Ban-Char500@Mag-(1:0) in Figure 1 (d) signifies the diffraction peaks observed at 2θ values of 23° and 42.5°, corresponding to the (002) and (101) planes of graphitic carbon, respectively, confirming the carbonaceous structure of the biochar.

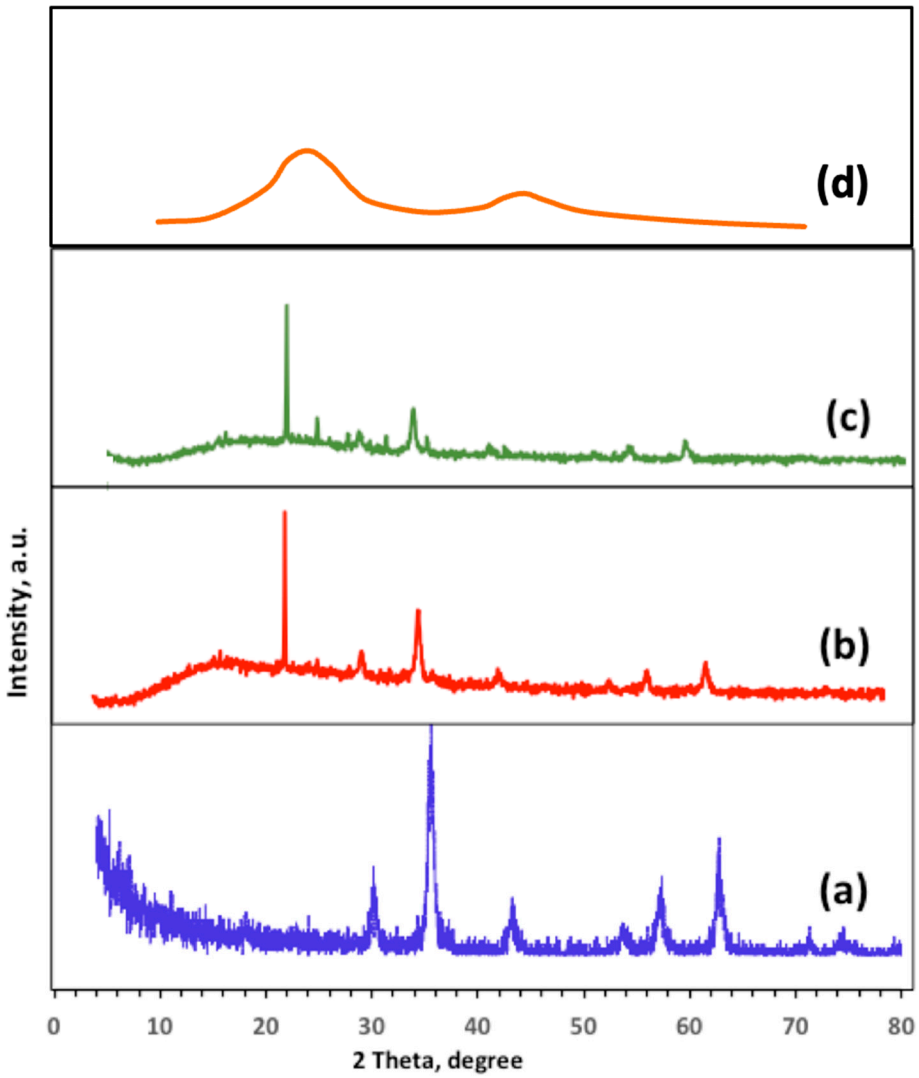


**Figure 1.** XRD of magnetite and banana biochar composites: (**a**) Ban-Char500@Mag-(0:1), (**b**) Ban-Char500@Mag-(1:1), (**c**) Ban-Char500@Mag-(2:1) and (**d**) Ban-Char500@Mag-(1:0).

FTIR

The FTIR result of the prepared composite Ban-Char500@Mag-(1:1) is illustrated in Figure 2. The data clearly confirms the presence of magnetite in the composite. Specifically, magnetite nanoparticles ($Fe_3O_4$) are signified by their characteristic Fe–O stretching bands at 585 and 460 $cm^{-1}$, while, simultaneously, surface O–H stretching is observed at 3400 $cm^{-1}$, together with the H–O–H bending mode of adsorbed water at 1635 $cm^{-1}$. Furthermore, organic bands, including aliphatic C–H stretching at 2920–2850 $cm^{-1}$, a carbonyl band around 1715 $cm^{-1}$, and aromatic C=C vibrations near 1600–1510 $cm^{-1}$, as well as strong C–O/C–O–C vibrations in the 1260–1030 $cm^{-1}$ region, are also present in the composite. Altogether, the coexistence of Fe–O bands with biochar-derived functionalities therefore provides evidence of successful coating and anchoring of magnetite on the carbonaceous surface. Hence, such results are consistent with interfacial interactions such as hydrogen bonding and electrostatic effect between surface hydroxyl/carboxyl groups and Fe sites.

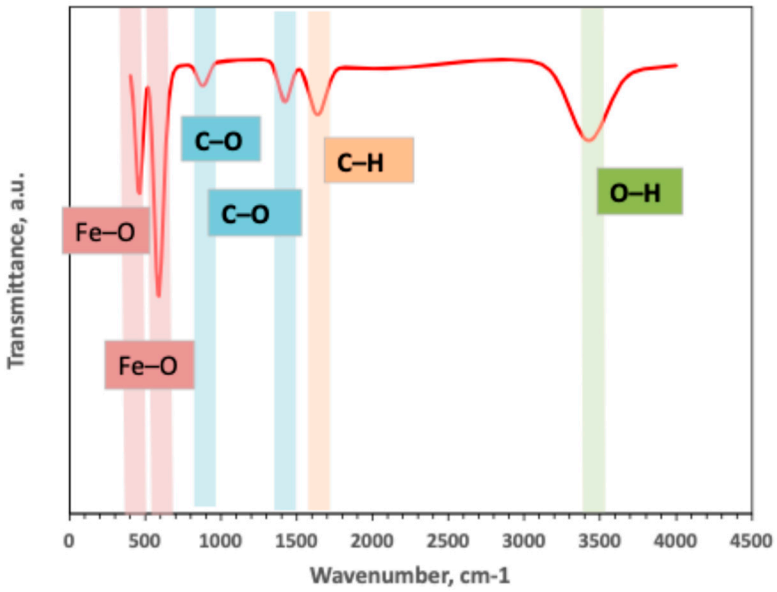


**Figure 2.** FTIR analysis of Ban-Char500@Mag-(1:1) composite material.

SEM and particle size distribution:

The SEM graph displayed in Figure 3a represents the magnetite nanoparticles and magnetite augmented with banana biochar with different proportions of (c) Ban-Char500@Mag-(1:1) and (e) Ban-Char500@Mag-(2:1). Ban-Char500@Mag-(0:1), which is related to magnetite nanoparticles, shows semi-spherical particle aggregates with a particle size distribution (Figure 3b) in an average of 6.8 nm. However, the images displayed in Figure 3c,e showed scattered grains with rough texture, as well as the presence of small semi-spherical-like particles that maintained the same particles of magnetite. Also, the particle size distribution is observed to be 9.77 nm (Figure 3d) and 10.42 nm (Figure 3f) for Ban-Char500@Mag-(1:1) and 6.83 nm for (e) Ban-Char500@Mag-(2:1), respectively. Thus, such images verify the presence of magnetite. Despite the presence of magnetite with Ban-Char500 biochar, the molecules are retaining their shape.

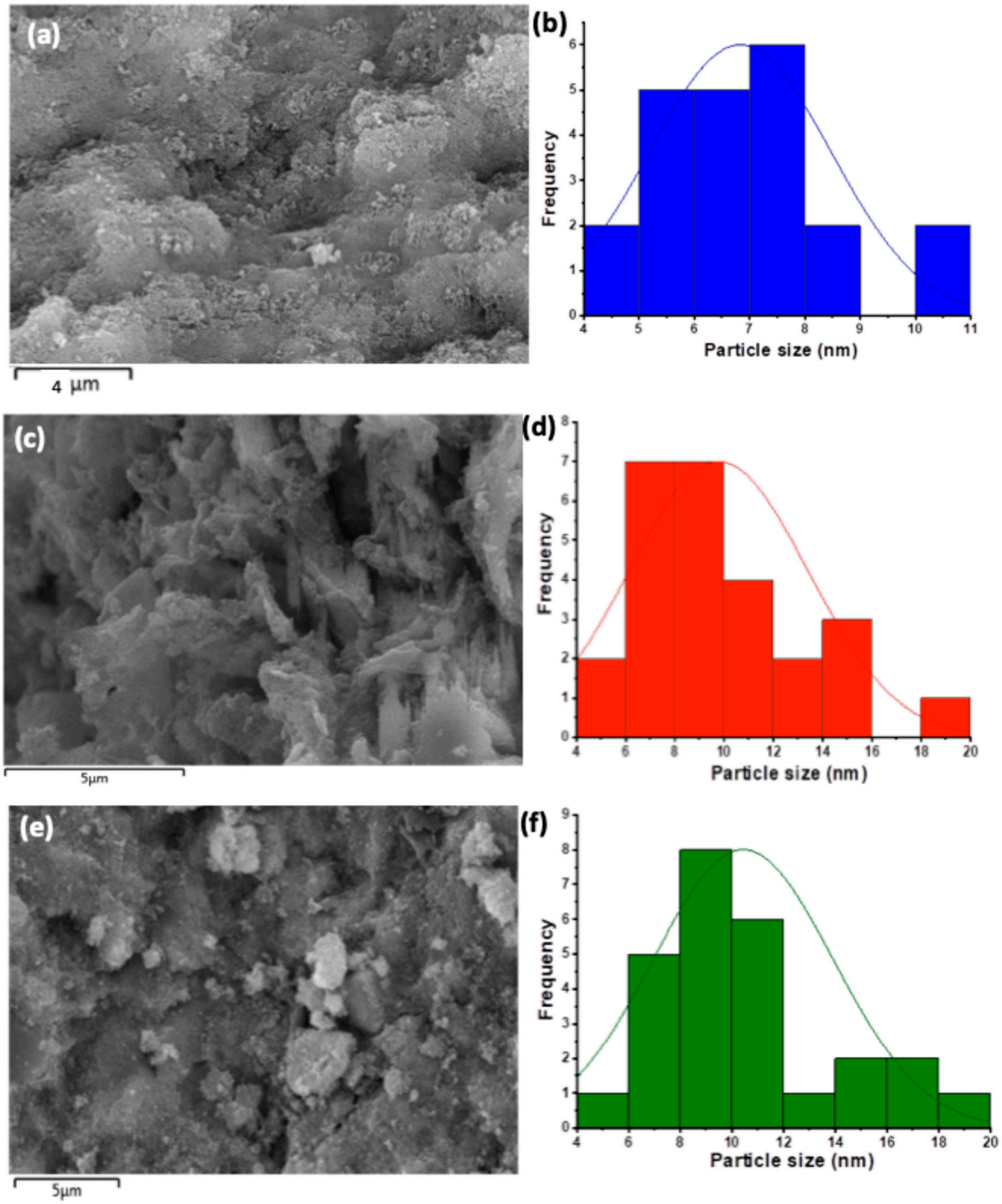


**Figure 3.** SEM images and particle size distribution of (**a**,**b**) Ban-Char500@Mag-(0:1), (**c**,**d**) Ban-Char500@Mag-(1:1) and (**e**,**f**) Ban-Char500@Mag-(2:1).

EDX and mapping

The Fe content in the composites was estimated using SEM–EDX analysis, which provides semi-quantitative values based on localized surface probing. As displayed in Figure

4a,c and their corresponding mapping graph of Figure 4b,d, the energy-dispersive X-ray spectroscopy (EDX) analysis of a selected area of the Ban-Char500@Mag-(1:1) and Ban-Char500@Mag-(2:1), respectively, verified the occurrence of O and Fe, elements found in magnetite, as well as the nitrogenous base and/or sugar elements (C, N, O) present. The corresponding EDX spectrum readily identified the presence of O and Fe, with the iron emission energy observed at 6.405 keV, which corresponds to the K$\alpha$ 1 peak. The assenting occurrence of all the above-mentioned elements in the synthesized Ban-Char500@Mag suggests the successful incorporation of magnetite with the banana-based biochar. Furthermore, the existence of Cl on the Ban-Char500@Mag-(1:1) sample in a low amount (0.05%) is most likely due to unreacted iron (II) and (III) chloride residues (i.e., magnetite precursors). Notably, such an amount might be trapped in the nanoparticle crystalline lattice during the co-precipitation synthesis.

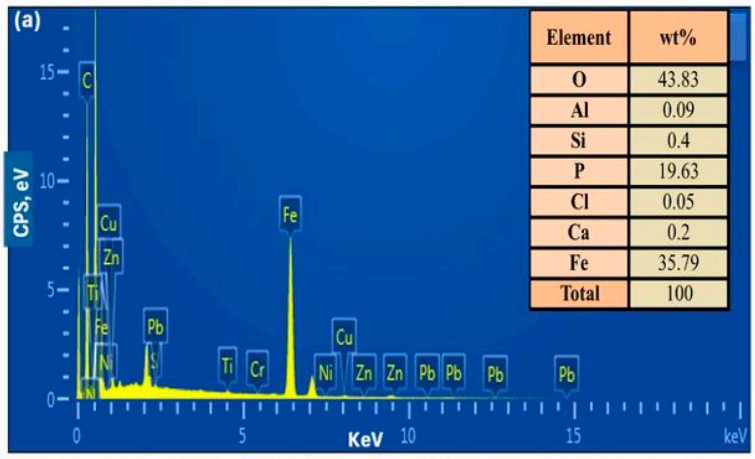
(a)
CPS, eV
KeV
keV
C
Cu
Zn
Ti
Fe
Pb
Ni
Cr
Element wt%
O 43.83
Al 0.09
Si 0.4
P 19.63
Cl 0.05
Ca 0.2
Fe 35.79
Total 100

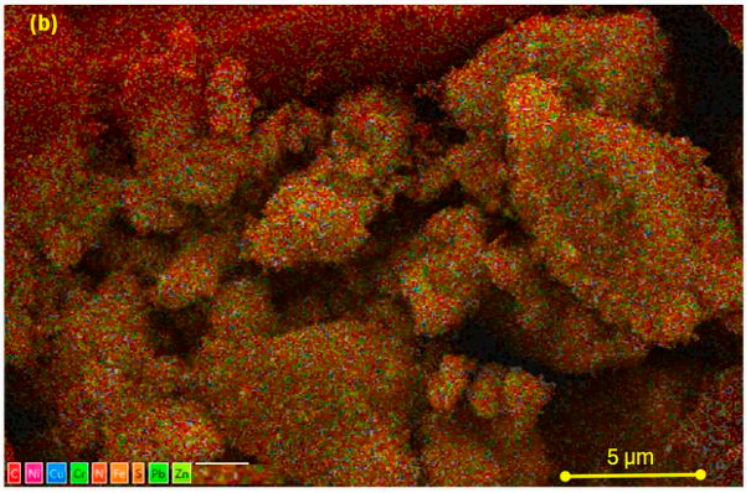
(b)
5 µm

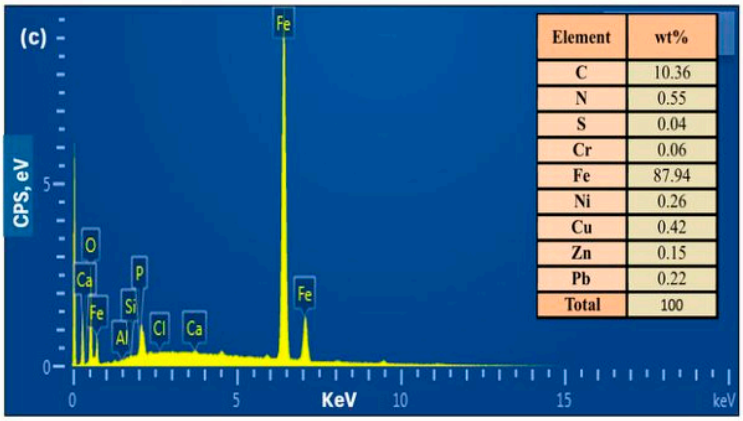
(c)
CPS, eV
KeV
keV
O
Ca
Fe
Si
P
Al
Cl
Ca
Fe
Element wt%
C 10.36
N 0.55
S 0.04
Cr 0.06
Fe 87.94
Ni 0.26
Cu 0.42
Zn 0.15
Pb 0.22
Total 100

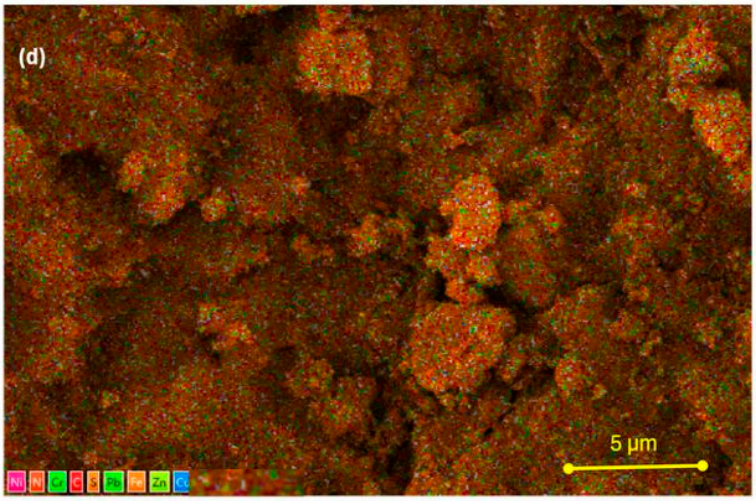
(d)
5 µm

**Figure 4.** (**a**,**b**) Ban-Char500@Mag-(1:1) and (**c**,**d**) Ban-Char500@Mag-(2:1) EDS mapping graphs.

### *2.2. Solar Radiation and Collector Analysis*

The parabolic trough solar collector represents the active constituent of the ultraviolet initiation technique that transfers the initiation process into the tubular reactor. A typical parabolic trough-collector type is used in this current work, as illustrated in the above-mentioned sections. The collector was placed facing south-west, according to the geographic location, and a tilt on the horizontal with an angle of 32° that suits the location. Results are from directly measured solar energy radiation intensity, in the place of experiment, during the summer season. Figure 5 illustrates that the maximum incident solar radiation recorded during the study reached 1015 W/m$^2$, representing the average solar intensity over the experimental period.

In the meantime, the ambient temperature is recorded through the study, to verify the solar intensity values. It is noteworthy to mention that temperatures and the solar intensity increases from the early morning to reach their maximum values around the solar noon. But the increased solar intensity begins to decline again later in the afternoon. Thus, the favorable conducting experimental time is around the solar noon [24].

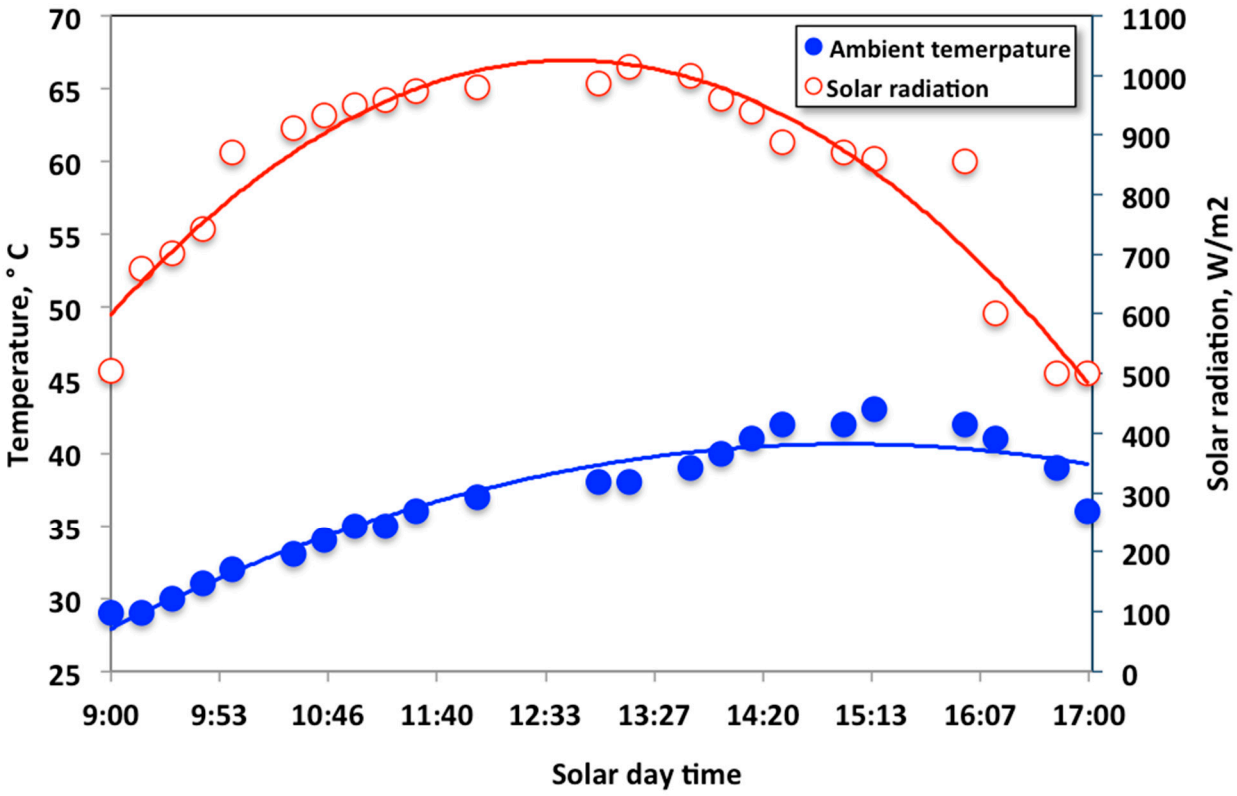


**Figure 5.** Thermal analysis of the photochemical parabolic trough collector versus time, showing the temperature profile and the solar intensity radiation.

### *2.3. Solar-Fenton Oxidation*

#### 2.3.1. Comparison of Illumination Time for Various Oxidation and Adsorption Systems

Initially, to evaluate and assess the suggested novel system, it is essential to compare it with various oxidation systems, and the data is displayed in Figure 6. To properly evaluate the proposed Char500@Mag-based solar-Fenton system, its performance was compared with adsorption and different oxidation pathways, as shown in Figure 6. The systems tested included the solo adsorption with Char500 biochar or adsorption with

magnetite alone, dark Fenton (without irradiation), $H_2O_2$/solar, Mag/solar, and the complete solar-Fenton system (Char500@Mag/$H_2O_2$/solar).

Acetaminophen removal is introduced for removing a pharmaceutical contaminate from aqueous effluent. Experiments were executed at various irradiance and oxidation times for all introduced systems including $H_2O_2$/solar, Mag/solar, and solar-Fenton based Ban-Char500@Mag-(1:1), and compared with the dark Fenton (without ultraviolet illumination), and the oxidation effectiveness rates were assessed. The data exhibited in Figure 6 at a natural wastewater pH condition (pH 6.8) revealed the effectiveness of the dual treatment represented in the Fenton (dual oxidation) system, augmenting solar photons as a source of initiation UV. The data represented a higher removal efficiency, corresponding to 95% of the solar-Fenton system in comparison to 45, 30 and 14% for the $H_2O_2$/solar, dark Fenton and Mag/solar systems, respectively. Such results verified both the roles of the solar system and the newly supplied Fenton source in conducting the oxidation reaction. Also, the reaction time that is required is only 60 min. However, it is noteworthy to mention that the first rapid rate of oxidation is identified within the initial 10 min of oxidation time. Afterwards, a steady oxidation rate within the next oxidation reaction is achieved.

The results presented in Figure 6 demonstrate that even though the dark Fenton showed a considerable low oxidation efficiency (30%) within one hour of reaction time, it could still oxidize acetaminophen. However, the solar-Fenton reaction could reach 95%, verifying the role of the presence of solar radiation. Also, the oxidation is stopped, and no further oxidation could occur; hydrogen peroxide is consumed through the reaction time and, thereby, no further •OH radicals are produced. This could be attributed to extra •OH radicals being generated in the dual solar-Fenton system. Furthermore, it is noteworthy to mention that the presence of Ban-Char500@Mag also helps in the acetaminophen molecules adsorption, as well as oxidation, since the presence of carbon acts as an adsorbent material. Consequently, when the vacant active sites of the Ban-Char500@Mag substance are saturated with the acetaminophen molecules, the propensity of the Char500@Mag material to adsorb more molecules is minimized. Such data are in accordance with the previously reported data in the literature, treating wastewater containing dye adsorption using a magnetite catalyst and adsorbent material. To sum up, the superior oxidation tendency is achieved within the initial reaction time, which might be linked to •OH radicals' speciation [28]. •OH radicals are traced through the catalytic decomposition of the $H_2O_2$ reagent by the Char500@Mag material.

Additionally, the results indicate that adsorption alone, whether with Char500 or magnetite, led to only limited acetaminophen removal (<10% within 60 min), confirming that physical uptake cannot account for the high removal observed in the composite system. It should be noted, however, that adsorption was evaluated only for 60 min under the present experimental conditions for direct comparison with the oxidation reactions. Extending the contact time, together with optimizing operational parameters (e.g., pH, dosage, and catalyst loading), could potentially enhance the adsorption performance and lead to higher acetaminophen removal efficiency.

Hence, the effective destruction of the acetaminophen molecules, which attacked through •OH radicals [55]. Consequently, the Char500@Mag composite containing magnetite possesses the advantage of being a sustainable recoverable solar photocatalyst material.

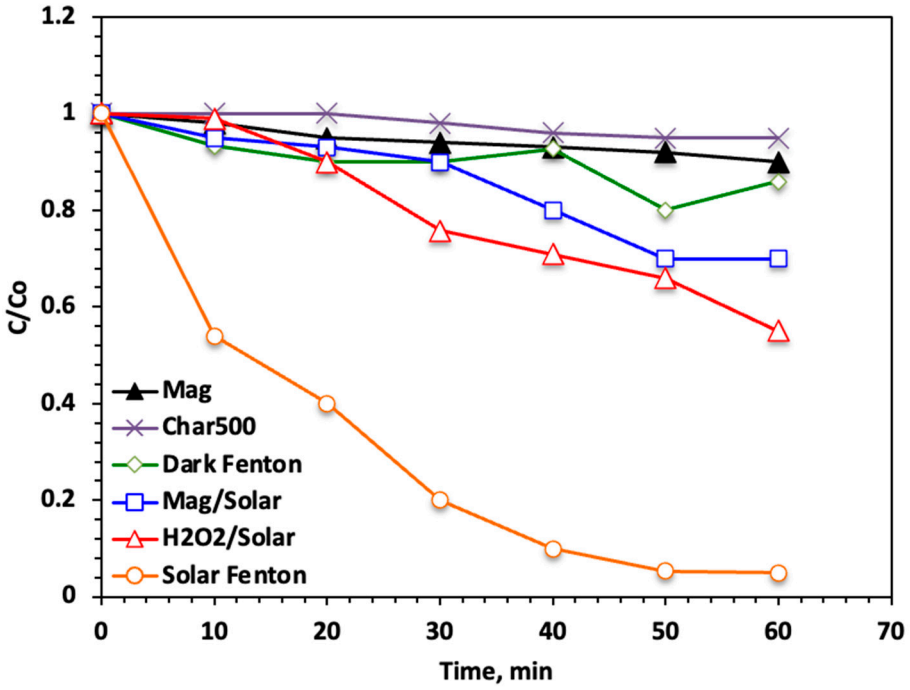


**Figure 6.** Effect of various oxidation and adsorption systems on the acetaminophen reaction time (Char500@Mag-(1:1) 10 mg/L; $H_2O_2$ 400 mg/L and pH 3.0).

2.3.2. Effect of Char500@Mag Composite Type

In the light of selecting the superior composite combination activity, it is essential to evaluate the ideal combination between magnetite and Char500-activated biochar biopolymer, Ban-Char500-Mag@-(1:0), Ban-Char500-Mag@-(0:1), Ban-Char500@Mag-(1:1) and Ban-Char500@Mag-(2:1)-based solar reaction, applied as as a source of the Fenton system. Hydrogen peroxide is supplemented to initiate the Fenton reaction. Various oxidation combinations' efficacy was assessed in terms of acetaminophen oxidation. Consequently, the initial doses are the catalyst in 10 mg/L and hydrogen peroxide of 100 mg/L, which were added to the wastewater at acidic wastewater pH conditions (pH 3.0), since the Fenton reaction might work at acidic conditions, as a modified solar-Fenton oxidation test, and the aqueous solution is subjected for solar irradiance in the photochemical reactor. The experiments are conducted around the solar noon at the time of the study.

The results displayed in Figure 7 validate that a high % of the acetaminophen removal is attained in the all applied systems, with a superior and shorter reaction time recorded for the corresponding system-based Ban-Char500@Mag-(1:1) system. It is essential to report that the initial oxidation time in all systems reveals greater oxidation effectiveness compared to exceeding the illumination time. The superiority of the solar-based catalyst is in the order of Ban-Char500@Mag-(1:1) >> Ban-Char500@Mag-(2:1) >> Ban-Char500@Mag-(0:1) >> Ban-Char500-Mag@-(1:0), which recorded 100, 98, 90 and 50%, respectively. This behavior can be explained by the influence of magnetite content in the reaction medium, as $Fe^{2+}/Fe^{3+}$ ions present in the composite act as the key reagents driving the solar-Fenton process. The banana peel-derived biochar serves as an effective adsorbent, and its combination with magnetite enhances the overall surface area of the material [18]. However, when the composite contains a higher proportion of biochar, adsorption becomes more dominant, while the catalytic role of magnetite is reduced. Consequently, the Ban-Char500@Mag (1:1) catalyst generates an excess of ·OH radicals, which synergistically supports both adsorption and oxidation, thereby improving system performance. In contrast, Ban-Char500@Mag (0:1), containing only biochar without magnetite, relies

solely on ·OH radical generation in the reaction medium, which results in lower efficiency compared to the combined oxidation–adsorption mechanism [44]. Thus, in the absence of magnetite, the composite functions primarily as a biochar –$H_2O_2$ system, where the degradation relies largely on hydrogen peroxide alone. This results in lower oxidation efficiency compared to systems incorporating magnetite, which play a crucial role in enhancing radical generation and overall performance.

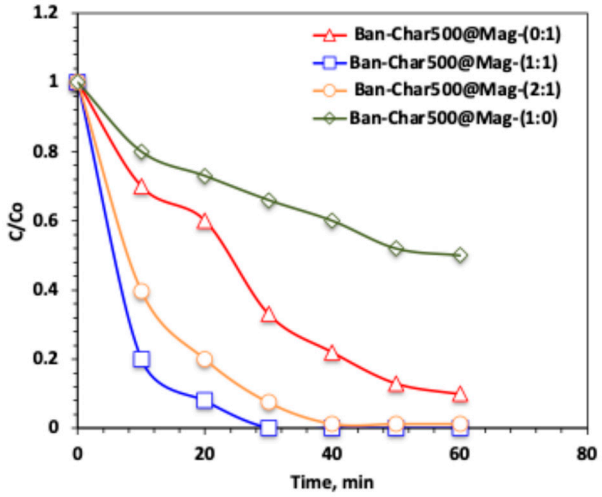


**Figure 7.** Effect of various Char500@Mag composites on the solar-Fenton oxidation system on acetaminophen removal.

### 2.3.3. Effect of Acetaminophen Loading

For catching the real scalar field applications, it is essential to study the pollutant loading on the performance of the solar oxidation suggested Ban-Char500@Mag-(1:1)-based Fenton oxidation. The initial acetaminophen concentration is varied to evaluate the pollutant loading on the performance of the solar catalytic-modified classical Fenton oxidation system. In this regard, the loading of acetaminophen is tested to examine $H_2O_2$/Ban-Char500@Mag/solar system oxidation capabilities. Figure 8 presents the effect of the modified Fenton oxidation process on acetaminophen at concentrations ranging from 50 to 200 ppm, while maintaining constant operating conditions (catalyst 10 mg/L, $H_2O_2$ 100 mg/L, and pH 3.0). The maximal acetaminophen removal efficacy is extended to a complete (100%) acetaminophen removal for the low concentrations, i.e., 50 ppm; when reached, it declines from 96 to 58 when the acetaminophen is increased gradually, from 100 to 200 ppm, respectively. This can be explained by the fact that the amounts of catalyst and $H_2O_2$ were kept constant in all experiments, while the acetaminophen load was progressively increased. As a result, the generated ·OH radicals were insufficient to achieve complete oxidation at higher pollutant concentrations.

Additionally, the available active vacant adsorbent sites on the composite of Mag (magnetite) and Ban-Char500@Mag (Banana biochar) are not sufficient to adsorb higher acetaminophen molecules. Additionally, the high acetaminophen molecules adsorbed on the Ban-Char500@Mag composite active sites might be causing the decline of the efficient hydroxyl radical's species' quantity. A similar exploration was previously reported in the literature by [19] in oxidizing organics through Fenton, initiated by the ultraviolet system.

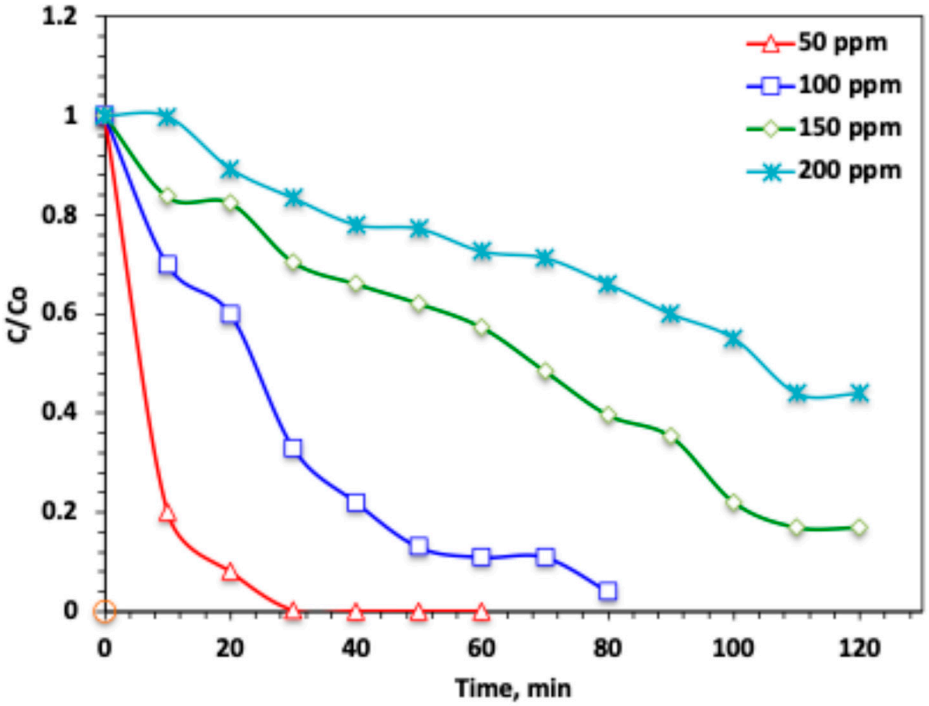


**Figure 8.** Effect of acetaminophen dose on the modified Char500@Mag Fenton oxidation system.

2.3.4. Catalyst Effect on Modified Solar-Fenton System

It is essential to investigate Char500@Mag as a catalyst and hydrogen peroxide ($H_2O_2$) reagent validity on the oxidation of acetaminophen by the suggested Fenton reaction, to proceed with an optimal reagent. Initially, Char500@Mag concentration is investigated, and the results are displayed in Figure 9. The effect of the dosage of Char500@Mag-(1:1) on the oxidation of acetaminophen was studied in the range of 5–40 mg/L. As the data illustrated in Figure 9 revealed a Char500@Mag increase from 5 to10 mg/L, the corresponding oxidation efficacy of acetaminophen increased from 67 to 100%, respectively, through 30 min of solar irradiance time. However, the further increase in adding Char500@Mag in the reaction medium results in a decline in the overall oxidation to 52 and 37% for 30 and 40 mg/L, respectively. The amount of Char500@Mag elevated is possibly postulated by extra active species for acetaminophen oxidation, and hence the results are an improvement in the oxidation proficiency.

However, when the Char500@Mag dosage is increased beyond a certain threshold (10 mg/L), the catalyst may precipitate in the reaction medium instead of effectively reacting with $H_2O_2$ to generate ·OH radicals. In addition, excess Char500@Mag particles can hinder the penetration of solar UV light into the medium, thereby reducing light absorption and diminishing oxidation efficiency. For this reason, a catalyst dosage of 10 mg/L was selected and applied in the subsequent experiments. This observed trend is consistent with previous reports involving various pollutants [24,33].

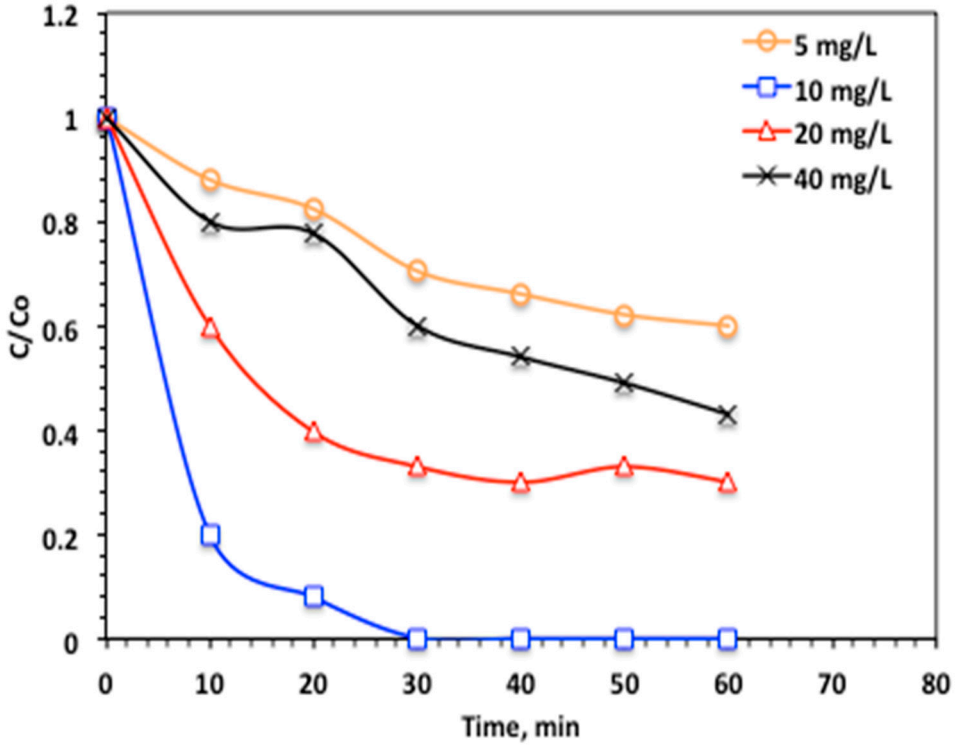


**Figure 9.** Effect of catalyst dose on the modified Char500@Mag Fenton oxidation system ($H_2O_2$ 100 mg/L and pH 3.0).

### 2.3.5. $H_2O_2$ Effect on Modified Solar-Fenton System

The influence of hydrogen peroxide on the oxidation of acetaminophen by the modified Fenton reaction catalyzed by Char500@Mag is exhibited in Figure 10. $H_2O_2$ increase results in an advance in the acetaminophen oxidation efficiency, resulting in a complete removal when the hydrogen peroxide is elevated from 50 to 100 mg/L. The mineralization rate reaches 100% of complete acetaminophen oxidation within 30 min of solar irradiance time. But this further increase, rather than 100 mg/L, is not favorable. Although the $H_2O_2$ is the source of the •OH radicals, in the Char500@Mag/$H_2O_2$/solar-Fenton system, notably, the elevation of the $H_2O_2$ reagent concentration from 100 to 400 mg/L results in a decline in acetaminophen oxidation that reaches 96 and 93% when the peroxide dose is increased to 200 and 400 mg/l, respectively.

This trend can be attributed to the enhanced generation of reactive species, particularly hydroxyl radicals (·OH), at certain concentrations where the balance between catalyst activity and oxidant availability favors radical production. However, when the $H_2O_2$ dose is further increased from 100 to 400 mg/L, additional radicals such as $O_2^{\bullet -}$ and $\bullet HO_2$ are formed in the reaction medium. These species exhibit significantly lower oxidation potentials compared to ·OH radicals, leading to a reduction in overall acetaminophen degradation efficiency. These findings are consistent with observations reported in previous studies [36,55]. Therefore, 100 mg/L can be considered the optimum $H_2O_2$ dosage for effective acetaminophen oxidation and removal from aqueous media.

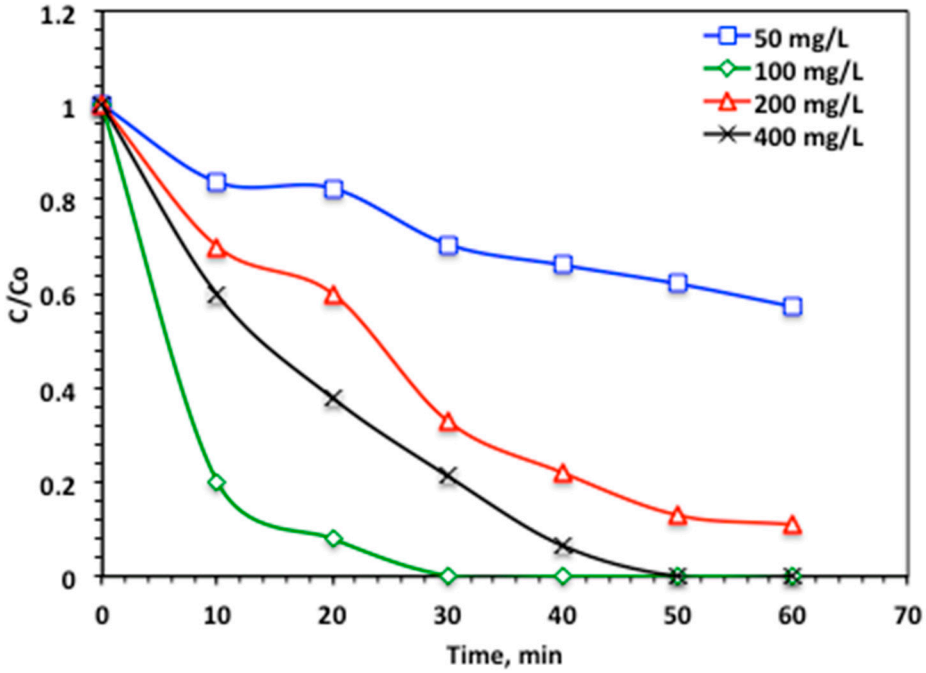


**Figure 10.** Effect of hydrogen peroxide dose on the modified Char500@Mag Fenton oxidation system (Char500@Mag-(1:1) 10 mg/L and pH 3.0).

2.3.6. pH Effect on Modified Solar-Fenton System

The effect of the operating pH on acetaminophen oxidation was examined by varying the initial pH of the aqueous medium from 3.0 to 8.0, while maintaining 100 mg/L hydrogen peroxide and 10 mg/L Char500@Mag catalyst under solar irradiation. The data exhibited in Figure 11 revealed that the acetaminophen oxidation rate is improved by a decline in pH value and when the optimal operating pH value is in acidic (3.0) conditions. But increasing the pH value results in a reduction in the acetaminophen oxidation rate. In particular, higher pH values in the alkaline range were found to be unfavorable, as they reduced the oxidation efficiency to only 78%. Notably, at pH 5.0, the system exhibited the lowest performance, with an oxidation rate of just 52% after 30 min of reaction.

Such an oxidation change, which is related to the pH value, can be clarified by the surface charge of the Char500@Mag catalyst. According to the previous work cited, the point of zero charge of Char500@Mag composite is recorded at about pH 7.2. The surface of the Char500@Mag catalyst might be charged in a negative or positive charge, due to the dissociation of the basic character of the catalyst at the point of zero charge. Hence, the change in the medium pH affects the surface charge of the catalyst, and thereby affects the catalytic and adsorption tendency. Hence, this could be illustrated by the presence of low electrostatic interactions among molecules of acetaminophen and the corresponding Char500@Mag molecules at the alkaline pH medium, whereby the oxidation rate is deduced [45,53].

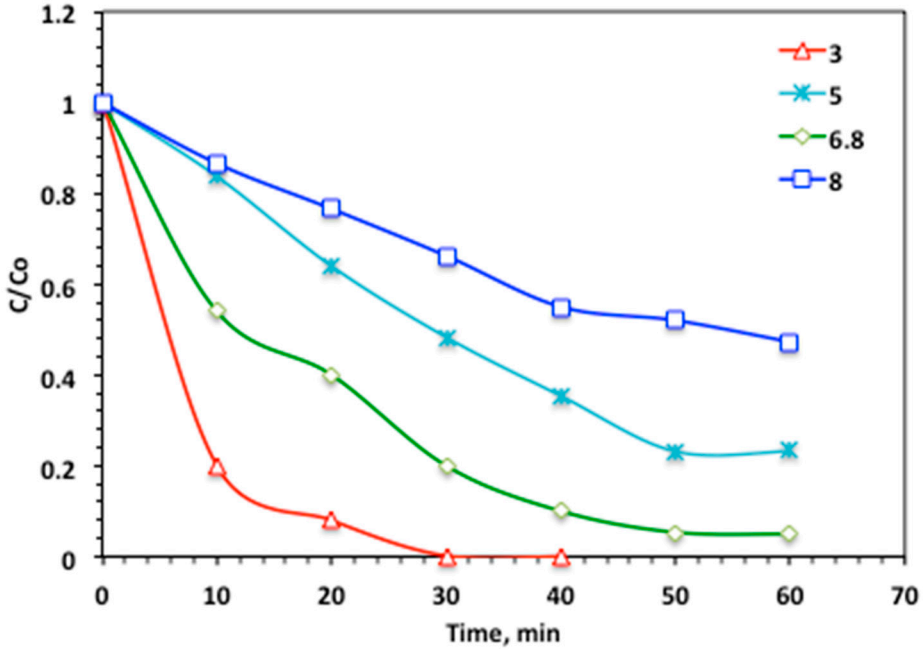


**Figure 11.** Effect of pH on the modified Char500@Mag Fenton oxidation system (Char500@Mag-(1:1) 10 mg/L and $H_2O_2$ 100 mg/L).

2.3.7. Temperature Effect on Modified Solar-Fenton System

To accomplish a real-life practical world, it is necessary to attain the effect of temperature, since it affects reaction rates, and the aqueous effluent might be discharged in various rates. From such a demonstration, the aqueous acetaminophen solution temperature is increased from 26 to 60 °C in the studied range, to evaluate the temperature influence on the oxidation reaction. The experimental data exposed in Figure 12 illustrated a reduction in the acetaminophen oxidation rate with the temperature elevation. A 100%, complete acetaminophen removal is achieved in almost 30 min of solar irradiance time at 26 °C. But further temperature elevation results in a decline in acetaminophen removal, ranging from 89 and 77 to 63%, with the gradual temperature increase of 40, 50 and 60 °C, respectively. Thus, at higher temperatures, there is a decline in the OH radicals rather than the low 26 °C room-temperature value. At elevated temperatures, a decline in hydroxyl radical production occurs, which negatively impacts the pollutant oxidation. This effect is further compounded by the thermal decomposition of $H_2O_2$ into $O_2$ and $H_2O$, thereby reducing the overall reaction rate. While some studies [23,33] have reported that higher temperatures promote ·OH radical formation, and consequently enhance oxidation efficiency, other investigations suggest that temperature exerts only a marginal influence on Fenton-based systems compared with other operational parameters. Therefore, it is verified by the literature that the higher reaction rate for the Fenton system is around room temperature (17–38 °C), which produces high-oxidative species.

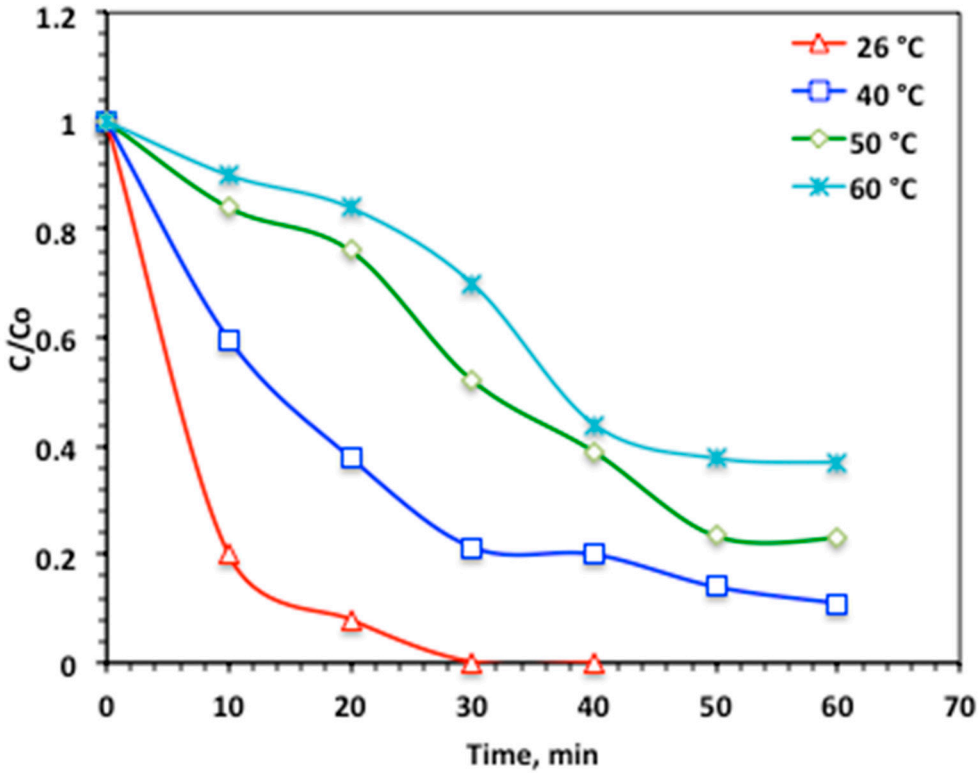


**Figure 12.** Effect of temperature on the modified Char500@Mag Fenton oxidation system.

2.3.8. Oxidation Kinetics

For further examining the oxidation reaction through the modified Char500@Mag-based solar-Fenton system, the oxidation kinetics is assessed. The kinetics calculations are accommodating an assessment of reactor design and system control that is essential for real-life applications. Thereby, it is assessing both underlying capital and operating expenses, to evaluate the total cost of treatment. Due to the heterogeneous nature of the Char500@Mag/$H_2O_2$ system for acetaminophen oxidation and the complexity of the intermediates generated during the reaction, it is not feasible to perform a detailed kinetic analysis for each individual pathway. Hence, the kinetic study represents the overall acetaminophen elimination. Acetaminophen removal as a function of time data through varied temperatures is fitted to the linear integrated equations forms for the three common kinetic models of $0^{th}$-, $1^{st}$-, and 2nd-order kinetics, according to their equations tabulated in Table 1. Such a plot is displayed in Figure 13, and the attained data is also displayed in Table 1.

Based on the comparison of correlation coefficients ($R^2$) from the kinetic plots, acetaminophen oxidation was found to follow first-order kinetics, as indicated by the highest $R^2$ values (0.95–0.96) compared to other kinetic models. Furthermore, the calculated half-life times ($t_{1/2}$) for the first-order model, as presented in Table 1, showed close agreement with the experimental results. These findings are consistent with previously reported studies [42], which also demonstrated that Fenton-based systems typically follow first-order reaction kinetics.

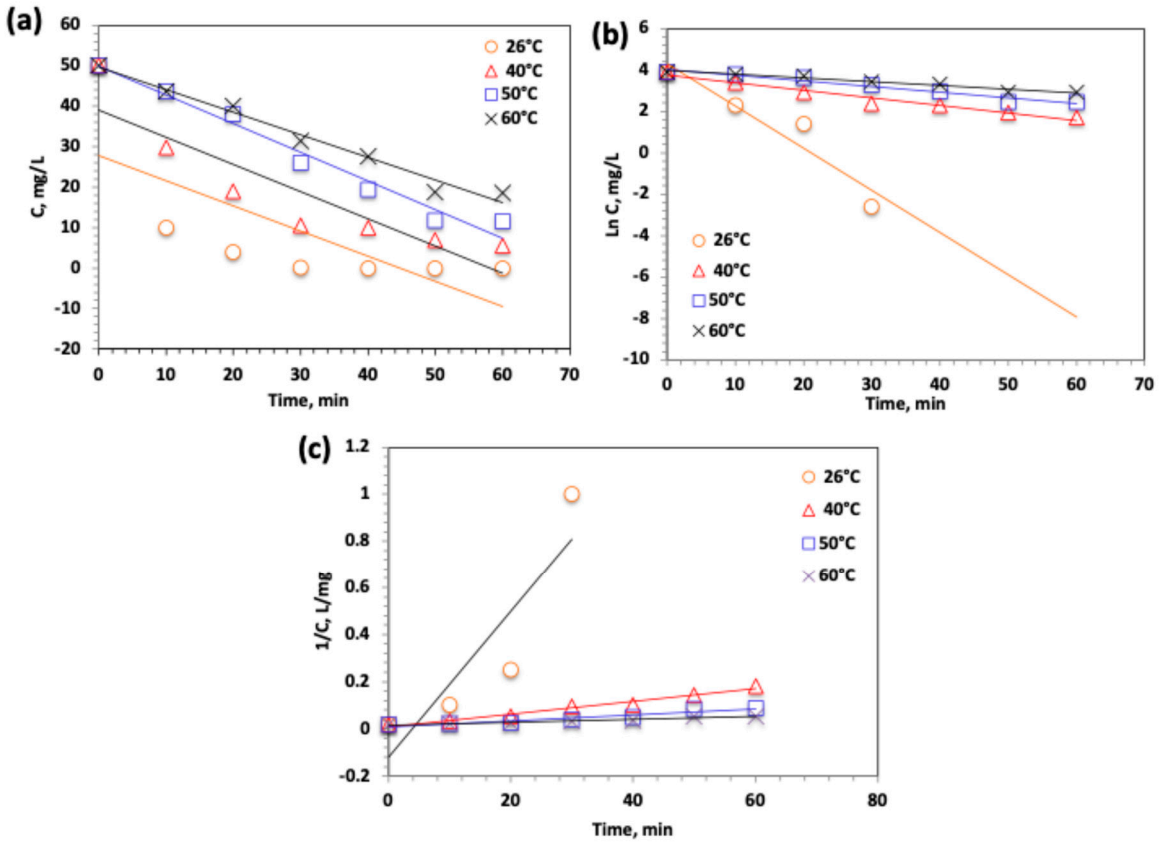


**Figure 13.** Plot of kinetic models of (**a**) Zero-order, (**b**) Pseudo-First-order and (**c**) Pseudo-Second-order for the modified Char500@Mag Fenton oxidation system.

**Table 1.** Parameters of kinetic models for acetaminophen oxidation by Char500@Mag-based solar-Fenton.

| Kinetic Model | Parameters | Values | | | |
|---|---|---|---|---|---|
| | | T, °C | | | |
| | | 26 °C | 40 °C | 50 °C | 60 °C |
| Zero-order ($C_t = C_o - k_0 t$) | $k_0$ (min$^{-1}$) | 0.62 | 0.67 | 0.71 | 0.56 |
| | $t_{1/2}$ (min) | 40.32 | 37.314 | 35.21 | 44.64 |
| | $R^2$ | 0.53 | 0.81 | 0.95 | 0.96 |
| Pseudo-First-order ($C_t = C_o - e^{k_1 t}$) | $k_1$ (min$^{-1}$) | 0.204 | 0.039 | 0.022 | 0.018 |
| | $t_{1/2}$ (min) | 38.5 | 31.5 | 17.76 | 3.39 |
| | $R^2$ | 0.95 | 0.96 | 0.95 | 0.96 |
| Pseudo-Second-order ($\left(\frac{1}{C_t}\right) = \left(\frac{1}{C_0}\right) - k_2 t$) | $k_2$ (L.mg$^{-1}$.min$^{-1}$) × 10$^{-2}$ | 0.4009 | 0.0027 | 0.0013 | 0.0006 |
| | $t_{1/2}$ (min) | 0.049 | 7.41 | 15.38538 | 33.34 |
| | $R^2$ | 0.62 | 0.67 | 0.71 | 0.56 |

Where *Co* and *Ct* are the concentrations at time 0 and time *t*; $k_0$, $k_1$ and $k_2$ are the kinetic constants of zero-and first- and second-order kinetics, respectively.

### 2.3.9. Activation Parameter Determination

To elucidate the influence of temperature on the oxidation process, activation parameters were assessed based on kinetic–thermodynamic analysis, and were evaluated based on the 1st-order kinetic model. Two complementary approaches were employed: the Arrhenius equation analysis for determining the apparent activation energy (Ea), and the Eyring transition state theory for estimating activation enthalpy ($\Delta H'$), entropy ($\Delta S'$), and

Gibbs free energy ($\Delta G'$) [52]. The linearized form of the Arrhenius equation is given according to the following equation:

$$\mathrm{Ln\,k_1} = \mathrm{ln\,A} - \frac{\mathrm{E_a}}{\mathrm{RT}} \quad (1)$$

where A is the pre-exponential factor constant; Ea is the energy of activation (kJ mol$^{-1}$); R is the gas constant (8.314 J mol$^{-1}$ K$^{-1}$); and T is temperature (K). The plot in Figure 14 displays the ln$k_1$ versus 1/T that is giving a linear relation, whereas its slope is corresponding to −Ea/R. In addition, the Eyring equation was applied:

$$\mathrm{k_1} = \frac{\mathrm{k_B T}}{\mathrm{h}} \mathrm{e}^{\left(-\frac{\Delta \mathrm{G}'}{\mathrm{RT}}\right)} \quad (2)$$

where kB is Boltzmann's constant and h is Planck's constant. From this relation, the enthalpy of activation was obtained using the following relation:

$$\Delta H' = E_a - RT \quad (3)$$

Moreover, the entropy of activation was derived from Equation (4):

$$\Delta S' = (\Delta H' - \Delta G')/T \quad (4)$$

Then, from the above-mentioned relations, the kinetic–thermodynamic data are calculated, and the data are tabulated in Table 2.

Based on these relations, the kinetic–thermodynamic activation parameters were independently evaluated at each temperature, and the results are summarized in Table 2. Minor variations in $\Delta H'$ and $\Delta\Delta S'$ across temperatures arise because the parameters were calculated separately for each experimental condition, reflecting the sensitivity of the Eyring relation to experimental data rather than true temperature dependence.

The results revealed that the Gibbs free energy of activation ($\Delta G'$) values were positive, as expected for chemical reactions, indicating the presence of an activation barrier that must be overcome for the reaction to proceed. The positive enthalpy of activation ($\Delta H'$) suggests an endothermic activation step, while the negative entropy of activation ($\Delta S'$) implies that the transition state is more ordered than the reactants. These findings are consistent with earlier reports on heterogeneous Fenton-like oxidation systems [45,52].

Although the overall oxidation of acetaminophen by the Char500@Mag/$H_2O_2$ system is thermodynamically feasible and exothermic, the observed decline in removal efficiency at elevated temperatures indicates that the process is not solely controlled by thermodynamics. Instead, kinetic factors (such as shorter residence times of reactive species) and mass transfer limitations may become dominant at higher temperatures, thereby reducing the net photocatalytic activity.

**Table 2.** Activation parameters for acetaminophen oxidation by Char500@Mag-based solar-Fenton.

| Parameter | T, °C | | | |
|---|---|---|---|---|
| | **26 °C** | **40 °C** | **50 °C** | **60 °C** |
| ΔG′ (kJ/mol) | 77.18 | 85.22 | 89.57 | 92.98 |
| ΔH′ (kJ/mol) | 57.71 | 57.60 | 57.51 | 57.43 |
| ΔS′ (J/mol K) | −65.11 | −88.26 | −99.23 | −106.75 |
| Ea (kJ/mol) | 60.20 | | | |

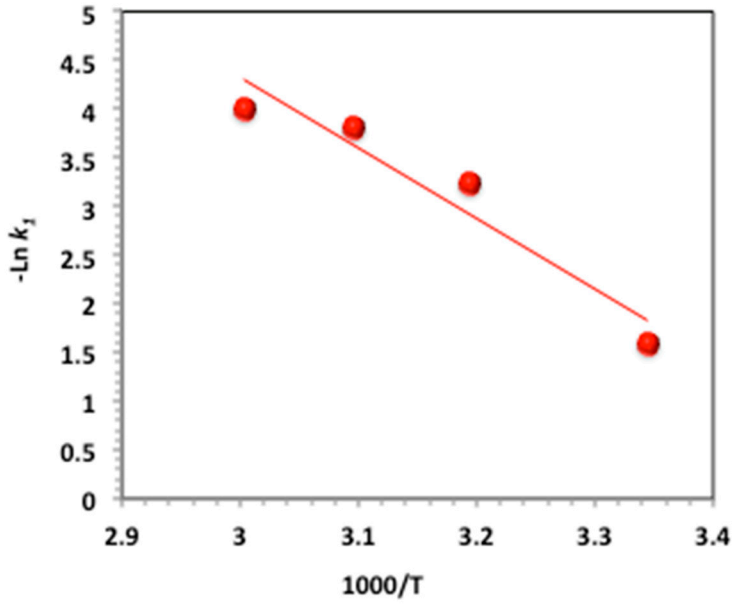


**Figure 14.** Plot of (−Ln $K_1$) vs. 1000/T.

2.3.10. Stability and Sustainability Assays

To verify the catalyst sustainability of Ban-Char500@Mag Fenton, the catalyst reuse is evaluated. Hence, after the oxidation test, the Ban-Char500@Mag is collected and then filtered prior to washing and cleaning with distilled water, with successive washes. The recovered catalyst is then oven-dried at 150 °C for one hour using an electric furnace. The successive use of the catalyst showed its sustainability for several cycles that could reach six cyclic uses. The data displayed in Figure 15 revealed that, compared to 100 removals for the fresh Ban-Char500@Mag use, continuing the oxidation under solar radiation reached 74% for the sixth cyclic use. Such a result is a considerably reasonable removal. This may be attributed to acetaminophen molecules occupying the active sites of the composite, thereby hindering further oxidation reactions. Previous cited data [33] are in accordance with such an investigation.

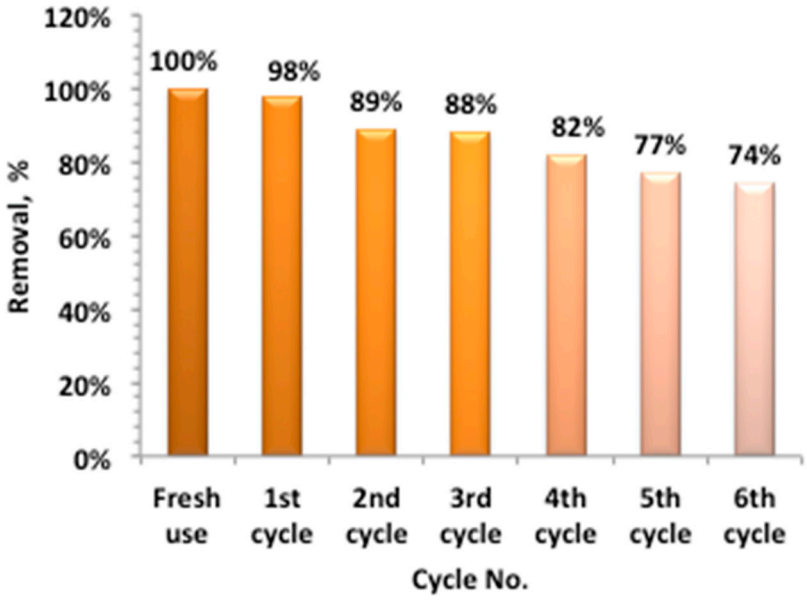


**Figure 15.** Catalyst recyclability activity on acetaminophen oxidation.

2.3.11. Study Compared with the Literature

The previously related cited work is compared to the current work; the comparison data is summarized in Table 3. The comparison is based on the operating time and the initiation source of activation of the Fenton system-type system for various pharmaceutical types contaminating aqueous media. The literature articles are examined, and the previous work is based on the dark Fenton or initiated systems through electro Fenton and/or ultraviolet initiation. Although the studies are based on the ultraviolet initiation, there is a lack of literature in using the renewable solar energy for initiation. Table 3 demonstrates that the solar-Fenton oxidation system in the present study achieved the complete removal of contaminants. Similar investigations reported in the literature have also shown high removal efficiencies in degrading various classes of pharmaceuticals, including antibiotics, anti-inflammatory drugs, and lipid-regulating (antilipemic) agents, effectively transforming them into non-toxic end-products. While alternative oxidation processes have likewise exhibited high efficiencies in eliminating such compounds, the solar-Fenton system remains a particularly effective and sustainable approach. It is significant to mention that the current work is based on a renewable costless energy-system facility in lesser reaction time. Hence, using solar energy exhibited a dual economically wise system and a clean renewable-energy efficient source. Additionally, it is noteworthy to mention that the introduced study suggests the use of a Fenton-based biochar/magnetite catalyst as a recoverable and recyclable material for sustainable use, since it is based on waste biochar material.

**Table 3.** Comparison of different Fenton systems for treating varied pharmaceuticals' wastewater.

| Fenton's Reaction Type/Catalyst * | Pharmaceutical Category | Oxidation (%) | Operating Conditions | Ref. |
|---|---|---|---|---|
| Electro/UV/Fenton/MSWCNTs–$FeCl_2$ | Anti-Inflammatory | 71% | pH: 5, MSWCNTs–$FeCl_2$: 0.05 M, oxidation time: 2 h | [55] |
| UV/Fenton (Fe/Cu/$TiO_2$) | Anti-Inflammatory | 41% | Cu/Fe: 1 g/L, oxidation time: 1 h | [56] |
| Dark Fenton/Fe-POM | Antibiotics | %97 | Fe-POM: 1 g/L, oxidation time: 0.2 h | [57] |
| Electro/UV/Fenton/$CuFeS_2$ | Antibiotics | 100% | pH: 3.0, $CuFeS_2$: 0.05 g/L, oxidation time: 0.25 h | [58] |
| Dark Fenton/MOF-Fe | Antilipemic agent | 62% | pH: 5.1, MOF-Fe: 0.05 g/L, oxidation time: 4 h | [59] |
| Electro/UV/Fenton/ZVI/C | Lipid-regulating | 94% | pH: 6.0, ZVI: 0.05 M, oxidation time: 1 h | [59] |
| Dark/Fe/C | Antibiotics | 95% | pH: 6.0, Fe/C: 1.0 g/L, oxidation time: 0.2 h | [60] |
| Electro/UV/Fenton/Fe | Antibiotics | 98% | pH: 3.0, Fe: 0.01 M, oxidation time: 1 h | [61] |
| Electro/UV/Fenton/Fe/C | Antibiotics | 70% | pH: 5.0, Fe/C: 0.05 M, oxidation time: 2 h | [62] |
| Electro/UV/Fenton/$FeS_2$ | Antibiotics | 99% | pH: 3.0, $FeS_2$: 0.05 M, oxidation time: 0.3 h | [63] |
| Electro/UV/Fenton/$Fe_2O_3$ | Antibiotics | 98% | pH: 3.0, $Fe_2O_3$: 0.01 M, oxidation time: 1 h | [64] |
| Electro/Fenton/$FeS_2$ | Antibiotic | 86% | pH: 4.0, $FeS_2$: 0.02 M, oxidation time: 6 h | [49] |
| Solar-Fenton/Ban-Char500@Mag-(1:1) | Antibiotic | 92% | pH: 3.0, Ban-Char500@Mag-(1:1): 10 mg/L, oxidation time: 0.5 h | Current work |

* ZVI: Zero Valent Iron; MOF: Metal Organic Frame; MSWCNTs: Metallic Single-Walled Carbon Nanotubes.

## 3. Materials and Methods

*3.1. Materials*

Wastewater:

Acetaminophen (AC) is selected to be a pharmaceutical model wastewater pollutant simulating the pharmaceutical discharge. The acetaminophen stock solution was prepared by dissolving the 1000 mg of the powder in one liter of distilled water, which is then

further diluted to the desired concentrations. Acetaminophen raw material is supplied by the Sigma-Aldrich Company. Sulfuric acid and/or sodium hydroxide is used to adjust the pH of the drug solution. All the used reagents and chemicals are of analytical grade and used as received, without further purification or treatment.

Organic waste:

*Musa sapientum*, which refers to banana peels, are collected from a local juice factory in Egypt. The material is transferred to the laboratory and then rinsed with water to remove any debris. Afterwards, it is left for air-drying prior to treatment.

### *3.2. Magnetic/Biochar from Musa Sapientum*

Banana peel biochar was prepared according to the previously described method [54], with some modifications. The material was washed with distilled water to remove any dust or impurities during the air-drying. Next, the material was then put in an oven at 80 °C overnight, to verify the complete dryness. Afterwards, the dried material was exposed for soaking overnight with phosphoric acid (60%). Then, the soaked material was subjected to an electrical furnace for semi-carbonization at a temperature of 200 °C for 4 h. The resultant dried biomass was cooled to room temperature and then carbonized in a furnace at 500 °C for 2 h for activation. The activated powder was then successively washed with distilled water to remove any remaining phosphoric acid in it by measuring the pH of the washing liquor that should reach neutral. Finally, the carbonized biochar was washed with 0.1 M NaOH solution followed by distilled water rinsing, to neutralize residual acidic groups, remove surface impurities, and enhance the exposure of active functional sites on the biochar surface. The subsequent material was dried overnight in an oven (105 °C) and exposed to ball mill-size reduction. The resultant treated and activated biochar is signified as Ban-Char500.

Consistently, the co-precipitation routine as a simple, economic, and high-yield method is applied to prepare the environmentally benign magnetite nanoparticles. In such a technique, 2 mol of $Fe_2(SO_4)_3$ and 1 mol of $Fe(SO_4)$ are used as a precursor to prepare such a substance. The two salts were mixed, then dissolved in 1.5 L of distilled water. About 8 mol of NaOH solution was added dropwise, while stirring till the pH of the solution reached 12.0 (alkaline pH). Subsequently, the mixture was exposed for stirring through heating (80 °C) and then a precipitate of nanoparticles formed. Subsequently, attained nanoparticles were then repeatedly washed using distilled water, in order to reach the neutral pH 7.0. The nanoparticles were then collected and exposed to electrical oven drying at 60 °C overnight. The resultant powder was labelled as "Mag".

Afterwards, mixed biochar with magnetite as a sustainable catalyst was prepared by mixing the biochar with the prepared magnetite nanoparticles and referred to as Ban-Char500@Mag. The mixture was added at different ratios, of 0:1, 1:1 and 2:1, and was signified as Ban-Char500-Mag@(0:1), Ban-Char500@Mag-(1:1) and Ban-Char500@Mag-(2:1), respectively. Consequently, the powder was stored in hermetic plastic bags till use. The preparation step is illustrated in the graphical illustration in Figure 16.

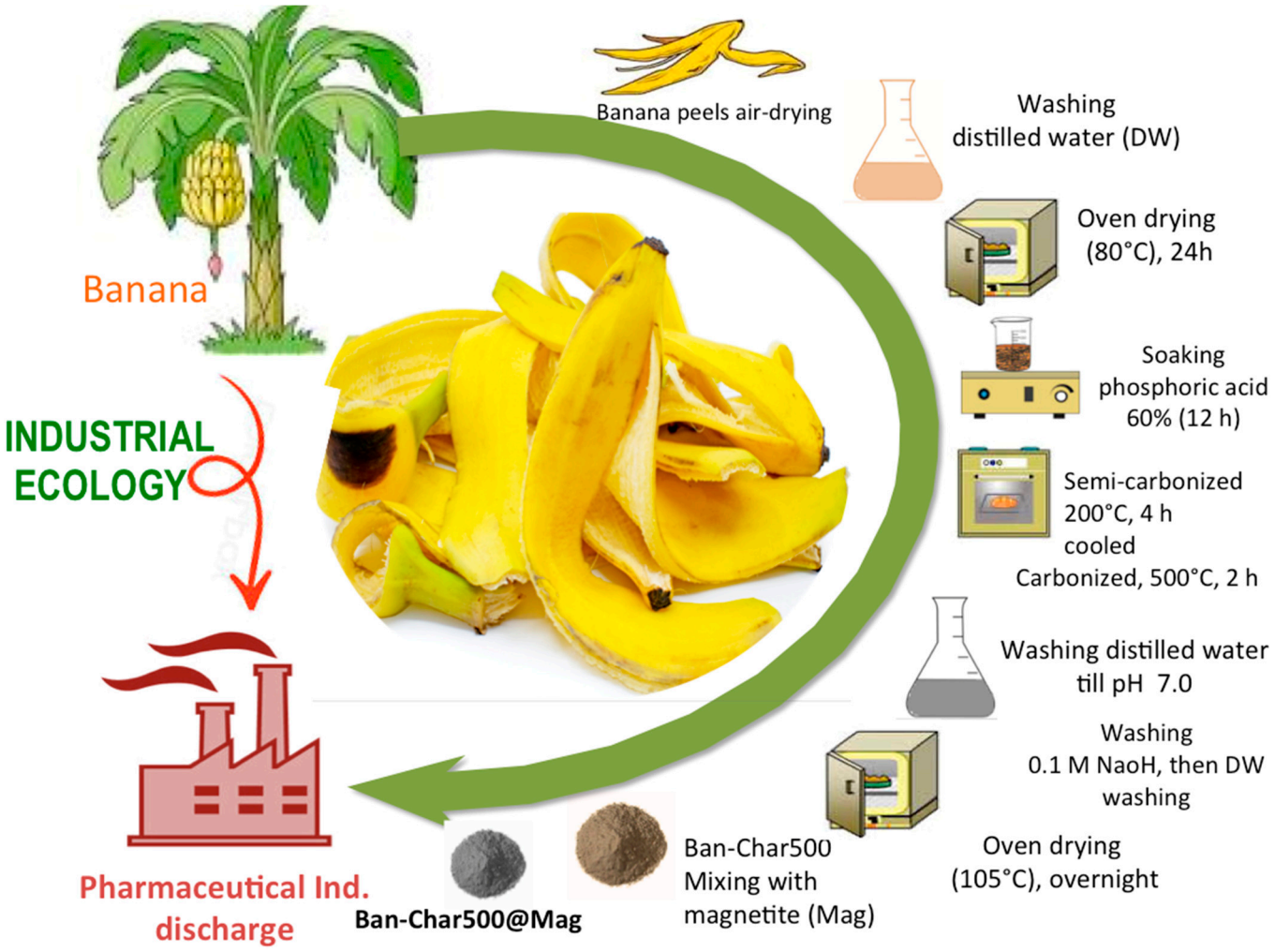


**Figure 16.** Schematic representation of the banana biochar/magnetite catalyst Ban-Char500-Mag.

### *3.3. Experimental Methodology and Analytical Determination*

A 1000 mL aliquot of the AC-water sample (at the studied concentrations in the range of 50 to 200 ppm) was exposed for stirring and left to stand under solar illumination in the solar photochemical reactor, to assure the Fenton photo oxidation reaction after the addition of the catalyst and hydrogen peroxide, to initiate the oxidation system. The pilot-scale experimental setup is mounted at the latitude (30°58′ N) and longitude (31°01′ E), which maximizes the solar radiation. The location generally enjoys dry mild and sunny days, especially in the summer season.

The photochemical reactor in a pilot-scale manner is designed with a parabolic trough collector to increase the parallel ray's incident solar radiation, and designed with a reflective sheet of stainless steel. The collector is framed facing the south, inclined from the ground according to the latitude of the location of study in Egypt (32°). Such a reactor consists of a tubular glass tube fabricated from silica glass fixed on a focal line of a collector to receive the reflected radiation from the parabola trough. The tubular reactor is connected to a feeding tank that includes the aliquot with the catalyst and hydrogen peroxide (30% w/v, supplied Alpha chemicals) to initiate the Fenton reaction. Then, the mixture is pumped to the reactor using a peristaltic dosing pump in a flow rate of 1800 mL/min. The schematic representation of the system is exhibited in Figure 17. Also, the solar radiation intensity is monitored using a solar meter (type: Eppley Black and White, Model: 8-48), which is placed closest to the parabolic trough collector at the time of the experiment.

The AC-water concentrations prior to and after the solar oxidation process were assessed through spectrophotometric analysis (UV–visible spectrophotometer type, model

Unico UV-2100 spectrophotometer, **UNICO,** USA) at the corresponding maximum wavelength of AC at 243 nm, at specific time intervals. All the experiments were performed on a pilot scale in the laboratory, the data collection is conducted in a triplicate manner, and the displayed results are the average of the three replicates.

Kinetic experiments were also conducted in a thermostatically controlled batch reactor (26–60 °C) equipped with a magnetic stirrer to ensure uniform mixing. A water-circulation system connected to a thermostatic bath was used to maintain the reaction temperature within ±1 °C at the desired set points. The initial acetaminophen concentration is 50 mg/L, whereas the fixed Char500@Mag-(1:1) dosage is 10 mg/L, and $H_2O_2$ at 10 mg/L. The initial solution pH was adjusted to 3.0, using dilute NaOH or $H_2SO_4$, prior to reaction. Then, samples were withdrawn at regular intervals and analyzed by UV–Vis spectrophotometry at regular intervals (0–60 min). Each experiment was repeated in triplicate, and mean values are reported. The experimental concentration-time data were evaluated by applying the integrated linear forms of zero-order, first-order, and second-order kinetic models, and the rate constants, correlation coefficients ($R^2$), and half-life values ($t_{1/2}$) were calculated accordingly.

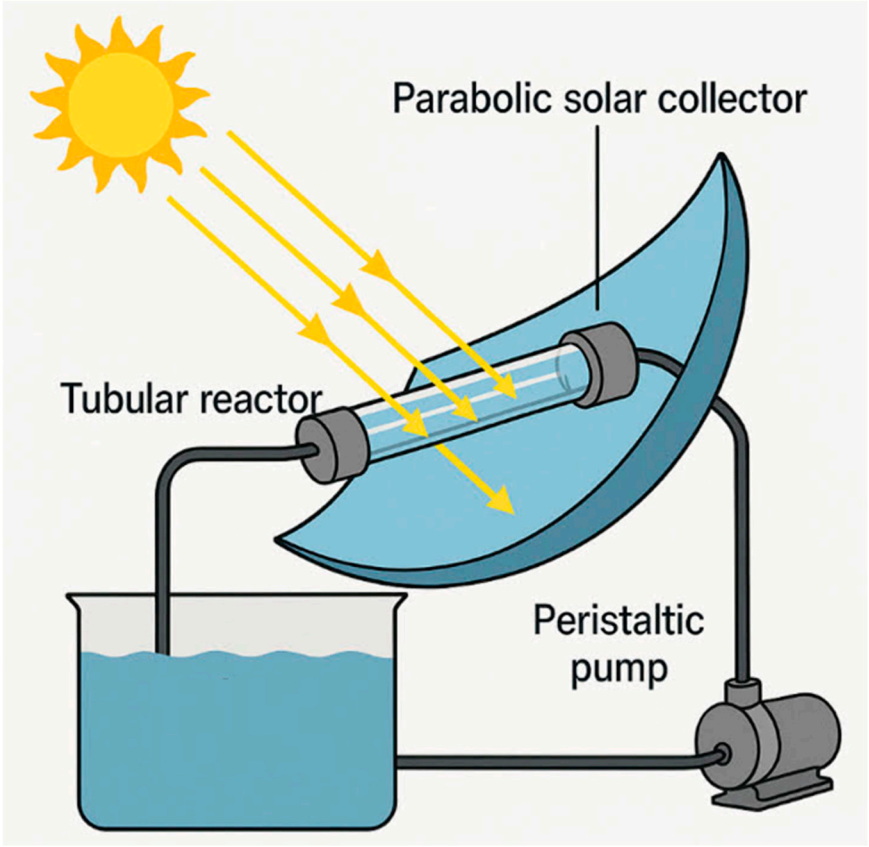


**Figure 17.** Schematic representation of the pilot-scale solar–photochemical oxidation system.

### *3.4. Ban-Char500-Mag Catalyst Characterizations*

The prepared Ban-Char500 samples were described through X-ray diffraction (XRD, D8-Find, Bruker, with CuK$\alpha$ radiation (1.5418 Å), Madison, WI, USA), working at a current of 40 MA, voltage of 40 kV, and step filter of 0.01° for crystalline nature. Furthermore, the morphology of such sample is also described by field emission–scanning electron microscopy (FE-SEM), using Quanta FEG 250, FEI Company, Hillsboro, OR, USA. Also, the dispersive X-ray spectroscopy (EDX) for elemental analysis is supplied using such an instrument (Quanta FEG 250). Also, Fourier-transform infrared (FTIR) analysis was performed in the region of 400–4000 $cm^{-1}$ wavenumber, using a Jasco FTIR-4100 spectrometer.

## 4. Conclusions

The Ban-Char500@Mag nanoparticle composite was synthesized through a straightforward route using waste banana peels as the precursor for biochar, augmented with the environmentally benign material magnetite. The composites were prepared at different magnetite-to-biochar ratios: Ban-Char500@Mag(0:1), Ban-Char500@Mag(1:1), and Ban-Char500@Mag(2:1). Structural and morphological analyses, confirmed by XRD diffractograms and SEM micrographs, revealed a moderately uniform distribution of magnetite nanoparticles on the Ban-Char500 biochar matrix. The resulting hybrid materials demonstrated multifunctional solar–photocatalytic activity, achieving up to 100% removal of acetaminophen, a model pharmaceutical contaminant, from aqueous effluents. Complete oxidation of acetaminophen was attained within only 30 min of solar irradiation in a photochemical reactor. Key operating parameters were optimized, and the reaction kinetics and thermodynamics were systematically investigated. The kinetic study showed that the oxidation system followed a first-order kinetic model with a global activation energy of 60.20 kJ/mol. Furthermore, recyclability tests confirmed the efficient recovery and sustained catalytic performance of the composite. Overall, this work highlights a green, cost-effective, and sustainable strategy for wastewater remediation, demonstrating the potential of waste-derived magnetite–biochar composites as highly efficient solar photocatalysts.

**Author Contributions:** Conceptualization, M.M.N., M.A.T., M.K.F. and H.A.N.; methodology, M.A.T.; investigation, M.A.T. and M.K.F.; writing—original draft, M.M.N. and H.A.N.; writing—review and editing, M.M.N., M.A.T., M.K.F. and H.A.N.; visualization, M.M.N. and H.A.N.; supervision, H.A.N. All authors have read and agreed to the published version of the manuscript.

**Funding:** The authors extend their appreciation to Prince Sattam bin Abdulaziz University for funding this research work through the project number (PSAU/2025/01/35045).

**Data Availability Statement:** Data available upon request.

**Conflicts of Interest:** The authors declare no conflicts of interest.

## References

1. Basheer, A.A. Chemical chiral pollution: Impact on the society and science and need of the regulations in the 21st century. *Chirality* **2018**, *30*, 402–406. https://doi.org/10.1002/chir.22808.
2. Bashir, A.; Malik, L.A.; Ahad, S.; Manzoor, T.; Bhat, M.A.; Dar, G.N.; Pandith, A.H. Removal of heavy metal ions from aqueous system by ion–exchange and biosorption methods. *Environ. Chem. Lett.* **2019**, *17*, 729–754. https://doi.org/10.1007/s10311-018-00828-y.
3. Bosio, G.N.; García Einschlag, F.S.; Carlos, L.; Mártire, D.O. Recent Advances in the Development of Novel Iron–Copper Bimetallic Photo Fenton Catalysts. *Catalysts* **2023**, *13*, 159. https://doi.org/10.3390/catal13010159.
4. Lai, Y.J.; Lee, D.J. Solid Mediator Z–Scheme Heterojunction Photocatalysis for Pollutant Oxidation in Water: Principles and Synthesis Perspectives. *J. Taiwan Inst. Chem. Eng.* **2021**, *125*, 88–114.
5. Zolfaghari, G.; Esmaili-Sari, A.; Anbia, M.; Younesi, H.; Ghasemian, M.B. A zinc oxide-coated nanoporous carbon adsorbent for lead removal from water: Optimization, equilibrium modeling, and kinetics studies. *Int. J. Environ. Sci. Technol.* **2013**, *10*, 325–340.
6. Beni, A.A.; Esmaeili, A. Biosorption, an efficient method for removing heavy metals from industrial effluents: A review. *Environ. Technol. Innov.* **2020**, *17*, 100503. https://doi.org/10.1016/j.eti.2019.100503.
7. Muthusamy, S.; Charles, J. Metal–organic framework of nanostructured polypyrrole incorporated with $TiO_2$ nanoparticles for supercapacitor electrode. *J. Mater. Sci. Mater. Electron.* **2021**, *32*, 7349–7365. https://doi.org/10.1007/s10854-021-05445-0
8. Ribeiro, E.; Plantard, G.; Teyssandier, F.; Maury, F.; Sadiki, N.; Chaumont, D.; Goetz, V. Activated-carbon/TiO2 composites preparation: An original grafting by milling approach for solar water treatment applications. *J. Environ. Chem. Eng.* **2020**, *8*, 104115. https://doi.org/10.1016/j.jece.2020.104115.

9. Muthukannan, V.; Praveen, K.; Natesan, B. Fabrication and characterization of magnetite/reduced graphene oxide composite incurred from iron ore tailings for high performance application. *Mater. Chem. Phys.* **2015**, *162*, 400–407.
10. Zhang, M.H.; Dong, H.; Zhao, L.; Wang, D.-X.; Meng, D. A Review on Fenton Process for OrganicWastewater Treatment Based on Optimization Perspective. *Sci. Total. Environ.* **2019**, *670*, 110–121.
11. Abdollahzadeh, H.; Fazlzadeh, M.; Afshin, S.; Arfaeinia, H.; Feizizadeh, A.; Poureshgh, Y.; Rashtbari, Y. Efficiency of activated carbon prepared from scrap tires magnetized by Fe3O4 nanoparticles: Characterisation and its application for removal of reactive blue19 from aquatic solutions. *Int. J. Environ. Anal. Chem.* **2020**, *102*, 1911–1925.
12. Tony, M.A.; Ali, I.A. Mechanistic implications of redox cycles solar reactions of recyclable layered double hydroxides nanoparticles for remazol brilliant abatement. *Int. J. Environ. Sci. Technol.* **2021**, *19*, 9843–9860.
13. Channei, D.; Thammaacheep, P.; Jannoey, P. Utilizing banana peel in conjunction with TiO2 photocatalyst for the efficient decolorization of malachite green. *Chem. Phys. Impact* **2024**, *8*, 100629.
14. Morales, A.E.; Mora, E.S.; Pal, U. Use of diffuse reflectance spectroscopy for optical characterization of un-supported nanostructures. *Rev. Mex. Física* **2007**, *53*, 18–22.
15. Maroudas, A.; Pandis, P.K.; Chatzopoulou, A.; Davellas, L.-R.; Sourkouni, G.; Argirusis, C. Synergetic decolorization of azo dyes using ultrasounds, photocatalysis and photo-fenton reaction. *Ultrason. Sonochemistry* **2021**, *71*, 105367.
16. Zhao, Y.Q.; Yang, Y. Extending the use of dewatered alum sludge as a P-trapping material in effluent purification: Study on two separate water treatment sludges. *J. Environ. Sci. Health Part A* **2010**, *45*, 1234–1239.
17. Tony, M.A.; Lin, L.-S. Iron Coated-Sand from Acid Mine Drainage Waste for Being a Catalytic Oxidant Towards Municipal Wastewater Remediation. *Int. J. Environ. Res.* **2021**, *15*, 191–201.
18. Wu, H.F.; Wang, J.P.; Duan, E.G.; Feng, Y.F.; Wan, Z.Y.; Wu, Y.X.; Lu, Y.Q. Study on the preparation of granular alum sludge adsorbent for phosphorus removal. *Water Sci. Technol.* **2019**, *79*, 2378–2386.
19. Abdou, K.A.; Mohammed, A.N.; Moselhy, W.; Farghali, A.A. Assessment of modified rice husk and sawdust as bio-adsorbent for heavy metals removal using nano particles in fish farm. *Asian J. Anim. Vet. Adv.* **2018**, *13*, 180–188.
20. Foroughi, M.; Chavoshi, S.; Bagheri, M.; Yetilmezsoy, K.; Samadi, M.T. Alum-based sludge (AbS) recycling for turbidity removal in drinking water treatment: An insight into statistical, technical, and health-related standpoints. *J. Mater. Cycles Waste Manag.* **2018**, *20*, 1999–2017.
21. Yin, Z.; Li, Y.; Song, T.; Bao, M.; Li, Y.; Lu, J.; Li, Y. Preparation of superhydrophobic magnetic sawdust for effective oil/water separation. *J. Clean. Prod.* **2020**, *253*, 120058.
22. Tony, M.A. Paradigms of homo/heterogonous Fenton systems incorporating 'Solar Energy' based on 'Emerging Pollutants' removal–challenges, advancements and visualized bibliometric analysis. *Int. J. Environ. Anal. Chem.* **2021**, *103*, 7877–7908.
23. Nabwey, Hossam A., and Maha A. Tony. "Thermal energy storage using a hybrid composite based on technical-grade paraffin-AP25 wax as a phase change material." *Nanomaterials* 13.19 (2023): 2635.
24. Hilder, M.; Winther-Jensen, O.; Winther-Jensen, B.; MacFarlane, D.R. Graphene/zinc nano-composites by electrochemical co-deposition. *Phys. Chem. Chem. Phys.* **2012**, *14*, 14034–14040.
25. Tauc, J. *Amorphous and Liquid Semiconductors*; Springer Science & Business Media: New York, NY, USA, 2012.
26. Kulkarni, S.A.; Sawadh, P.S.; Palei, P.K.; Kokate, K.K. Effect of synthesis route on the structural, optical and magnetic properties of $Fe_3O_4$ nanoparticles. *Ceram. Int.* **2014**, *40*, 1945–1949.
27. Amir, M.; Baykal, A.; Güner, S.; Güngüneş, H.; Sözeri, H. Magneto-optical investigation and hyperfine interactions of copper substituted Fe3O4 nanoparticles. *Ceram. Int.* **2016**, *42*, 5650–5658.
28. Bachan, N.; Asha, A.; Jeyarani, W.J.; Kumar, D.A.; Shyla, J.M. A Comparative investigation on the structural, optical and electrical properties of SiO2–Fe3O4 core–shell nanostructures with their single components. *Acta Metall. Sin. (Engl. Lett.)* **2015**, *28*, 1317–1325.
29. Ge, J.; Zhang, Q.; Zhang, T.; Yin, Y. Core–satellite nanocomposite catalysts protected by a porous silica shell: Controllable reactivity, high stability, and magnetic recyclability. *Angew. Chem.* **2008**, *120*, 9056–9060.
30. Ahangaran, F.; Hassanzadeh, A.; Nouri, S. Surface modification of $Fe_3O_4$@$SiO_2$ microsphere by silane coupling agent. *Int. Nano Lett.* **2013**, *3*, 23.
31. Zhang, H.; Niu, Z.; Liu, Z.; Wen, Z.; Li, W.; Wang, X.; Wu, W. Equilibrium, kinetic and thermodynamic studies of adsorption of Th (IV) from aqueous solution onto kaolin. *J. Radioanal. Nucl. Chem.* **2015**, *303*, 87–97.
32. Aroke, U.O.; Abdulkarim, A.; Ogubunka, R.O. Fourier-transform infrared characterization of kaolin, granite, bentonite and barite. *ATBU J. Environ. Technol.* **2013**, *6*, 42–53.

33. Chang, C.-F.; Wu, Y.-L.; Hou, S.-S. Preparation and characterization of superparamagnetic nanocomposites of aluminosilicate/silica/magnetite. *Colloids Surf. A Physicochem. Eng. Asp.* **2009**, *336*, 159–166.
34. Chen, C.-W. *Magnetism and Metallurgy of Soft Magnetic Materials*; Courier Corporation: Chelmsford, MA, USA, 2013.
35. James, R.D. Magnetic alloys break the rules. *Nature* **2015**, *521*, 298–299.
36. Guo, S.; Dan, Z.; Duan, N.; Chen, G.; Gao, W.; Zhao, W. Zn (II), Pb (II), and Cd (II) adsorption from aqueous solution by magnetic silica gel: Preparation, characterization, and adsorption. *Environ. Sci. Pollut. Res.* **2018**, *25*, 30938–30948.
37. Raut-Jadhav, S.; Pinjari, D.V.; Saini, D.R.; Sonawane, S.H.; Pandit, A.B. Intensification of degradation of methomyl (carbamate group pesticide) by using the combination of ultrasonic cavitation and process intensifying additives. *Ultrason. Sonochemistry* **2016**, *31*, 135–142.
38. Nichela, D.A.; Berkovic, A.M.; Costante, M.R.; Juliarena, M.P.; Einschlag, F.S.G. Nitrobenzene degradation in Fenton-like systems using Cu (II) as catalyst. Comparison between Cu (II)-and Fe (III)-based systems. *Chem. Eng. J.* **2013**, *228*, 1148–1157.
39. Singh, C.; Chaudhary, R.; Gandhi, K. Preliminary study on optimization of pH, oxidant and catalyst dose for high COD content: Solar parabolic trough collector. *Iran. J. Environ. Health Sci. Eng.* **2013**, *10*, 13.
40. Shanmugam, B.K.; Easwaran, S.N.; Mohanakrishnan, A.S.; Kalyanaraman, C.; Mahadevan, S. Biodegradation of tannery dye effluent using Fenton's reagent and bacterial consortium: A biocalorimetric investigation. *J. Environ. Manag.* **2019**, *242*, 106–113.
41. Toosi, F.S.; Hosseiny, M.; Joghataei, A.; Toosi, F.S. The application of SiO2 nanoparticles for anionic dye removal from aqueous solution. *Arch. Hyg. Sci.* **2017**, *6*, 136–144.
42. Buthiyappan, A.; Raman, A.A.A.; Daud, W.M.A.W. Development of an advanced chemical oxidation wastewater treatment system for the batik industry in Malaysia. *RSC Adv.* **2016**, *6*, 25222–25241.
43. Ahmadi, M.; Behin, J.; Mahnam, A.R. Kinetics and thermodynamics of peroxydisulfate oxidation of Reactive Yellow 84. *J. Saudi Chem. Soc.* **2016**, *20*, 644–650.
44. Do, Q.C.; Kim, D.-G.; Ko, S.-O. Catalytic activity enhancement of a $Fe_3O_4$@$SiO_2$ yolk-shell structure for oxidative degradation of acetaminophen by decoration with copper. *J. Clean. Prod.* **2018**, *172*, 1243–1253.
45. Huang, X.; Nan, Z. Formation of octahedron-shaped $ZnFe_2O_4$/$SiO_2$ with yolk–shell structure. *J. Phys. Chem. Solids 2020*, *141*, 109410.
46. Phan, T.T.N.; Nikoloski, A.N.; Bahri, P.A.; Li, D. Facile fabrication of perovskite-incorporated hierarchically mesoporous/macroporous silica for efficient photoassisted-Fenton degradation of dye. *Appl. Surf. Sci.* **2019**, *491*, 488–496.
47. Nour, Manasik M., Maha A. Tony, and Hossam A. Nabwey. "Heterogeneous fenton oxidation with natural clay for textile levafix dark blue dye removal from aqueous effluent." *Applied Sciences* 13.15 (2023): 8948.
48. Hassan, E. A., Tony, M. A., Nabwey, H. A., & Awad, M. M. (2023). Potential of the Biomass Waste Originating from Saccharum officinarum as a Fenton Precursor for the Efficient Oxidation of Azo Dye from an Aqueous Stream. *Processes*, *11*(5), 1394.
49. Ye, Z.; Schukraft, G.E.; L'Hermitte, A.; Xiong, Y.; Brillas, E.; Petit, C.; Sirés, I. Mechanism and stability of an Fe-based 2D MOF during the photoelectro-Fenton treatment of organic micropollutants under UVA and visible light irradiation. *Water Res.* **2020**, *184*, 115986.
50. Hassan, E. A., Tony, M. A., Nabwey, H. A., & Awad, M. M. (2023). Management of Agricultural Water Containing Acetimidothioic Acid Pesticide through Catalytic Oxidation to Facilitate Reclaimed Water Recycling for Sustainable Food Production. *Processes*, *11*(3), 792.
51. Shoorangiz, M., Nikoo, M. R., Salari, M., Rakhshandehroo, G. R., & Sadegh, M. (2019). Optimized electro-Fenton process with sacrificial stainless steel anode for degradation/mineralization of ciprofloxacin. *Process Safety and Environmental Protection*, *132*, 340-350.
52. Thiam, A.; Salazar, R.; Brillas, E.; Sirés, I. In-situ dosage of $Fe^{2+}$ catalyst using natural pyrite for thiamphenicol mineralization by photoelectro-Fenton process. *J. Environ. Manag.* **2020**, *270*, 110835.
53. Soliman, E.M.; Ahmed, S.A.; Fadl, A.A. Adsorptive removal of oil spill from sea water surface using magnetic wood sawdust as a novel nano-composite synthesized via microwave approach. *J. Environ. Health* **2020**, *18*, 79–90.
54. Srinivasakannan, C.; Bakar, M.Z.A. Production of activated carbon from rubber wood sawdust. *Biomass Bioenergy* **2004**, *27*, 89–96.
55. Sadeghi, M.; Mehdinejad, M.H.; Mengelizadeh, N.; Mahdavi, Y.; Pourzamani, H.; Hajizadeh, Y.; Zare, M.R. Degradation of diclofenac by heterogeneous electro-Fenton process using magnetic single-walled carbon nanotubes as a catalyst. *J. Water Process Eng.* **2019**, *31*, 100852.
56. Tamuly, C.; Saikia, I.; Hazarika, M.; Das, M. Reduction of aromatic nitro compounds catalyzed by Biogenic CuO nanoparticles, *RSC Adv.* **2014**, *4*, 53229–53236.

57. Jiang, J.; Wang, X.; Liu, Y.; Ma, Y.; Li, T.; Lin, Y.; Xie, T.; Dong, S. Photo-Fenton degradation of emerging pollutants over Fe-POM nanoparticle/porous and ultrathin g-C3N4 nanosheet with rich nitrogen defect: Degradation mechanism, pathways, and products toxicity assessment. *Appl. Catal. B Environ.* **2020**, *278*, 119349.
58. Collins, D.; Luxton, T.; Kumar, N.; Shah, S.; Walker, V.K.; Shah, V. Assessing the impact of copper and zinc oxide nanoparticles on soil: A field study. *PLoS ONE* **2012**, *7*, e42663.
59. Midander, K.; Cronholm, P.; Karlsson, H.L.; Elihn, K.; Mo, L.; Leygraf, C.; Wallinder, I.O. Surface characteristics, copper release, and toxicity of nano- and micrometer-sized copper and copper(II) oxide particles: A cross-disciplinary study. *Small* **2009**, *5*, 389–399.
60. Scherrer, P. Bestimmung der Grösseundderinneren Struktur von Kolloidteilchen mittels Röntgenstrahlen. *Nachr. Ges. Wiss. Göttingen* **1918**, *26*, 98–100.
61. Nguyen, T.T.; Huynh, K.A.; Padungthon, S.; Pranudta, A.; Amonpattaratkit, P.; Tran, L.B.; Phan, P.T.; Nguyen, N.H. Synthesis of natural flowerlike iron-alum oxide with special interaction of Fe-Si-Al oxides as an effective catalyst for heterogeneous Fenton process. *J. Environ. Chem. Eng.* **2021**, *9*, 105732.
62. Molina, C.B.; Sanz-Santos, E.; Boukhemkhem, A.; Bedia, J.; Belver, C.; Rodriguez, J.J. Removal of emerging pollutants in aqueous phase by heterogeneous Fenton and photo-Fenton with $Fe_2O_3$-$TiO_2$-clay heterostructures. *Environ. Sci. Pollut. Res.* **2020**, *27*, 38434.
63. Droguett, C.; Salazar, R.; Brillas, E.; Sirés, I.; Carlesi, C.; Marco, J.F.; Thiam, A. Treatment of antibiotic cephalexin by heterogeneous electrochemical Fenton-based processes using chalcopyrite as sustainable catalyst. *Sci. Total Environ.* **2020**, *740*, 140154.
64. Kalantary, R.R.; Farzadkia, M.; Kermani, M.; Rahmatinia, M. Heterogeneous electro-Fenton process by Nano-$Fe_3O_4$ for catalytic degradation of amoxicillin: Process optimization using response surface methodology. *J. Environ. Chem. Eng.* **2018**, *6*, 4644.